Multimedia Tools and Applications (2023) 82:39157–39210
https://doi.org/10.1007/s11042-023-15029-1

Bio-medical imaging (X-ray, CT, ultrasound, ECG), genome sequences applications of deep neural network and machine learning in diagnosis, detection, classification, and segmentation of COVID-19: a Meta-analysis & systematic review

Yogesh H. Bhosale[1] · K. Sridhar Patnaik[1]

Received: 12 May 2022 / Revised: 1 February 2023 / Accepted: 27 February 2023 /
Published online: 15 March 2023

Abstract
This review investigates how Deep Machine Learning (DML) has dealt with the Covid-19 epidemic and provides recommendations for future Covid-19 research. Despite the fact that vaccines for this epidemic have been developed, DL methods have proven to be a valuable asset in radiologists' arsenals for the automated assessment of Covid-19. This detailed review debates the techniques and applications developed for Covid-19 findings using DL systems. It also provides insights into notable datasets used to train neural networks, data partitioning, and various performance measurement metrics. The PRISMA taxonomy has been formed based on pretrained(45 systems) and hybrid/custom(17 systems) models with radiography modalities. A total of 62 systems with respect to X-ray(32), CT(19), ultrasound(7), ECG(2), and genome sequence(2) based modalities as taxonomy are selected from the studied articles. We originate by valuing the present phase of DL and conclude with significant limitations. The restrictions contain incomprehensibility, simplification measures, learning from incomplete labeled data, and data secrecy. Moreover, DML can be utilized to detect and classify Covid-19 from other COPD illnesses. The proposed literature review has found many DL-based systems to fight against Covid19. We expect this article will assist in speeding up the procedure of DL for Covid-19 researchers, including medical, radiology technicians, and data engineers.

Keywords Pattern / feature extraction · Bio-medical imaging · Deep machine learning · Diagnosis · Classification · Radiography imaging(X-ray · CT · Ultrasound · ECG) · Deep neural network · Chronic obstructive pulmonary diseases (COPD)

✉ Yogesh H. Bhosale
yogeshbhosale988@gmail.com

[1] Computer Science and Engineering Department, Birla Institute of Technology, Mesra, Ranchi, India

Abbreviations

ANN	Artificial Neural Networks
ARDS	Acute Respiratory Distress Syndrome
AUC	Area Under the Curve
CAM	Class Activation Map
CNN	Convolutional Neural Network
COPD	Chronic Obstructive Pulmonary Diseases
Covid-19	Corona Virus Disease-2019
CT	Computed Tomography
CXR	Chest X-ray
DCNN	Deep Convolutional Neural Network
DL	Deep Learning
DT	Decision Tree
DWT	Discrete Wavelet Transform
ECG	Electrocardiography
GAN	Generative Adversarial Network
GGO	Ground Glass Opacity
KNN	K-Nearest Neighbours
LR	logistic regression
LSTM	Long Short-Term Memory
LUS	Lung Ultrasound
MERS-CoV	Middle East Respiratory Syndrome Coronavirus
MI	Myocardial Infarction
MLP	Multi-Layer Perceptron
mRMR	minimum Redundancy and Maximum Relevance
NBC	Naive Bayes Classifiers
NPV	Negative Predictive Value
PCR	Polymerase Chain Reaction
PPV	Positive Predictive Value
ResNet	Residual Network
RF	Random Forest
RFE	Recursive Feature Elimination
RNN	Recurrent Neural Networks
RT-PCR	Reverse Transcription-Polymerase Chain Reaction
SARS	Severe Acute Respiratory Syndrome
SARS-COV-2	Severe Acute Respiratory Syndrome Coronavirus 2
STN	Spatial Transformer Networks
SVM	Support Vector Machines
VGG	Visual Geometry Group
WHO	World Health Organization

1 Introduction

Covid-19 originated from Wuhan, China [29] and has affected all the country's citizens worldwide since December 2019 [3, 6]. As of January 25, 2023, a total of 664,873,023 affirmed patients of Covid-19 were conveyed to the WHO worldwide, including 6,724,248

deaths. As of January 23, 2023, a total of 13,156,047,747 doses of vaccine had been directed [134, 162]. As per Ministry HFW Covid Report [105], until January 27, 2023, the Covid-19 active cases were 1896, total deaths were 530,739, and 2,203,602,459 doses of vaccine had been directed to citizens of India itself. According to a recent BBC article [153], COVID19 totaled 59,938 fatalities in China between December 8 to January 12, 2023, and the amount of confirmed cases has climbed. The effectiveness of Sinovac and Sinopharm, the two primary vaccinations produced in China, against Omicron, the greatest common strain, is under question(Due to China's refusal to use vaccinations from other nations) [153]. However, the situation is different in other nations throughout the world, where the fatality rate and the number of positive cases have sharply decreased.

The Covid-19 pandemic affects worldwide health and causes economic disasters [73, 99]. Detecting the novel coronavirus [147] from the human body is remarkably important and vital in the primary phases. Currently, the global healthcare community uses RT-PCR [18, 68, 133] tests and is looking for alternate ways to detect Covid-19 from radiology images. WHO recommends that all corona infection diagnoses be validated using RT-PCR [69]. Unfortunately, the earlier days of screening using RT-PCR require hours to days [32], which is a threat for COVID19 individuals. But As a result, radiological imagery is conducted initially with the early identification of COVID19, followed by the RT-PCR examination to assist clinicians in finalizing real-time confirmation [22]. However, at present, the time cost and money cost of RT-PCR are lower than that of CT, but the sensitivity of CT is higher not only in recognizing COVID19 but also COPD [19]. COVID-19 is diagnosed using multiple healthcare visualization tools: X-ray [103], CT-scan [10], and Ultrasound [139], ECG-trace images [20]. The period between contamination [18] and the appearance of the first Covid19 symptoms [22] can extend up to 15-days [46]. In the nonexistence of regular signs such as fever, the choice of a radiograph image of the lung has a comparatively excellent facility to sense the illness [131]. The percentage portion of the lungs affected due to Covid-19 (determined by using appropriate deep transfer learning CNN variants [45]) can be found efficiently using radiological images like X-ray, CT, and ultrasound. Although maximum patients have mild symptoms of Covid-19, physicians must apply the same caring methods to isolate, treat and monitor [163].

Apart from RT-PCR, the primary method that can be adopted to identify COVID19 is an X-ray, ECG, and ultrasound technique that has the benefit of becoming cheaper and low-risk in terms of radiation harm to patients [140, 146]. Finding Covid-19 via the X-ray and Ultrasound technique is a reasonably complex job. A radiographer should carefully examine those radiographs to identify the white patches comprising liquid and abscess [18, 22], which would be time-consuming and difficult. Various disorders, including respiratory TB, might be misdiagnosed as Covid-19 by radiologists or expert physicians [119].

The X-ray and ultrasound have a significant erroneous ratio to the radiologist [18]. Hence, CT scans could be employed for better accurate identification [8, 17]. However, CT picture costs are considerably higher than X-ray and Ultrasound [94]. Multiple sections are presented from each patient accused of carrying Covid-19 at the moment of CT-scan collection. Large CT-scan samples demand a strenuous effort from practitioners and doctors to confirm Covid-19 [14, 76, 78–80, 92, 100, 113, 128, 135, 137, 145, 166].

The infection can be categorized by lung GGO (Ground Glass Opacity) in initial phases, trailed by paving and growing consolidation. So, these outcomes are directed to the increased demand for CT machines in China, mainly in the Hubei region, ultimately flattering a competent prognosis instrument [57]. The study [60] stated that the Covid-19 affected patients' CT scan images found abnormalities on chest CT-scan, wherein all showed multifocal patchy GGOs particularly close to

the marginal segments of the lungs. The study [16] states that distinctive lung CT results are 2-sided lung parenchymal GGO and consolidative pulmonic opacities.

In past centuries, implementations of DML in the healthcare domain have resulted in several types of research aimed at diagnosing various illnesses, like brain cancer from MRI [51, 156], brain diseases from electroencephalography [4, 50], mammary disease from digital mammograms [106], and respiratory illnesses like Covid-19 from X-ray [131], CT-scan [115], ultrasound [27], ECG [20], DNA [61]. DL, a subgroup of Machine Learning(ML), has shifted aspirations in several fields of artificial intelligence(AI) in information analytics over the previous decade by achieving the highest precision [47] in a variety of jobs, particularly in the health domain [102]. This indicates that the proposed review is best suitable for recognizing Covid-19 from different imaging modalities and genome sequences.

The large population of countries like China and India suffered from Covid-19 vaccination because of mismanagement. To address such issues, the best blockchain technology can be practiced to develop and circulate Covid-19 vaccines [163], for example, delivering a patient's regular medicine to the patient's doorstep or nearby local pharmacy center. Along with DL, the IoT, Big Data, AI, and blockchain technologies play a crucial role in the Covid-19 healthcare domain, like observing, investigating, finding, and preventing using the Covid-19 system. IoT examples include virtual clinics-PingAn [127], real-time tracing, and live information in numerous virtual databases worldwide [70]. Big data provides business modeling on pharmaceutical supplies for various medications, demonstrating infection movement, possible evolution, and spread zones. Examples of AI include the discovery of Covid-19 through radiography chest imaging [96] and the use of a medical chatbot to answer public inquiries about Covid-19 Arogya-Setu [65]. Blockchain examples like life cover assertions from Covid-associated disease and demise. The following precise research questions (RQ) motivated our study:

RQ 1: How can DL be utilized to detect and classify Covid-19?
RQ 2: What are the possible diagnosis methods using radiography images?
RQ 3: Which radiography modality(X-ray, CT, Ultrasound, ECG) and genome sequence is primarily used to detect Covid-19 using DL-based pretrained, custom/hybrid models?
RQ 4: The technical challenges and limitations associated with Covid-19 detection using DL?

This review article emphasizes on DL based technical results for Covid-19 detection, with the following key contributions:

- This is the principal survey reviewing Covid-19 applications exclusively in the domain of Deep Learning.
- A systematic review with advanced development of Covid-19 diagnosis methods built on DL using radiography modalities(CT, ultrasound, X-ray, paper-based ECG trace imaging) and COVID19 genomic sequencing.
- Presents the analysis work and related information in a rich, brief, and manageable form, considering key elements, such as the dataset used for experimentation, partitioning methods, and recommended diagnosis and performance analysis frameworks.
- Establish the taxonomy of the examined research to have a better insight into the developments.
- To emphasize and debate the complex aspects of existing DL-based Covid-19 assessment systems.

- Presents scrutiny of the critical results in DL techniques, including analytical and technical information of experimental setups and performance benchmark metrics explained in theoretical and practical aspects.
- Recommendation for upcoming research to advance accurate and scalable Covid-19 identification systems.

Following is the breakdown of the upcoming sections. The taxonomy of important study directions, categorizing the researched systems using neural networks, imaging modality-based classification tasks, and datasets with practical understanding and quantitative analytical diagrams are described in Section 3. Section 3 to 7 enlightens the recent relative work for Covid-19 diagnosis using radiography images and genome sequencing with pre-trained, hybrid, and custom-trained experimental architecture with DTL. Benchmark performance evaluation metrics used in this study are listed in Section 8.2.1. Section 8 focuses on the discussion (strengths), challenges (weaknesses), and future plan. The survey boundaries are given in Section 9. Finally, Section 10 has been concluded with closing remarks. The list abbreviations are as follows:

2 Literature taxonomy of Covid-19 detection, diagnosis, and classification systems

WoS, Scopus, MEDLINE, PubMed Central(PMC), DOAJ, Google Scholar, etc., are the indexing databases used for searching Covid-19 research articles in this review study, which assesses the usage of DL-based Covid19 recognition and classification systems. These systems were utilized for diagnostic imaging to solve serious illnesses and analyze the performance of each method. The primary goal of this study is to implement the literature review, which entailed searching for significant published articles using PRISMA. Until Sept. 2021, a query study was conducted using "Deep Learning," "Covid-19," "Diagnosis," "Radiological Imaging" and "genome sequencing" which were the most common keywords used for obtaining 348 articles (Fig. 1). Ninety-five articles have been ultimately chosen (the remaining articles were not considered because of excluding criteria and their provided performance metrics were not in the acceptable range). Finally, 42 studies were included for qualitative synthesis, and the remaining 20 studies were selected for quantitative analysis. This comprehensive analysis aimed to provide a general overview of the researched studies that relied on DL with radiography pictures published. Figure 2 shows several databases that selected the number of papers published on DML techniques for Covid19.

2.1 Deep neural network architecture

Pre-trained and custom models are used for taxonomies distribution of DL networks. Automatic detection of Covid19 system has been developed using pre-trained DL architectures, such as CNN [72], RNN [7], GAN [98], hybrid networks like CNN-RNN and CNN-LSTM [7], and custom-built frameworks DeCovNet [164], AnamNet [124], AD3D-MIL [59], PQIS-Net [93], Puldi-COVID [19], etc.

Apart from heavy and large-scale networks like ResNet [75], GoogleNet [165], NasNetLarge [19], Inception [142], VBNet [171], DenseNet [24], Xception [101], etc. the lightweight feature space also plays a vital role in the detection of Covid19 like AnamNet

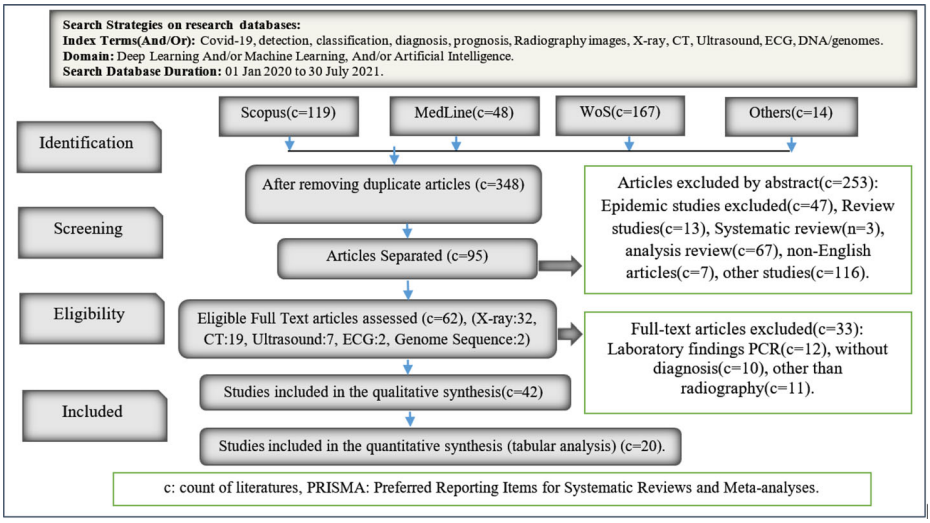

Fig. 1 Inclusion and exclusion flowchart criteria adapted for literature review PRISMA

[124], MNas3DNet41 [62], LEDNet, UNet++ [26], Reg-STN [139], LDC-NET [21] and DeepLabV3+ [26] that is simple to install on machines with limited resources. Also, the custom lightweight models are SPPCOVID-Net [2] and shallow-CNN [109]. DenseNet, AlexNet [112], GoogleNet [10], Inception [111], ResNet [46], SqueezeNet, VGG [98], and Xception were recognized to be the DL structure designs employed for the assessment of Covid19 from radiological images [132].

Figure 3 shows the general flowchart used for Covid19 diagnosis containing data preprocessing, DML models, operations, and final results. Methods accomplished in preprocessing step are removing noisy/blurry samples, rescaling, labeling, augmentation, normalization, data partitioning(train, val, test set), etc. The training sample is emplyed to produce a specific model(pretrained, custom/hybrid) for feature extraction [138, 141], segmentation, and

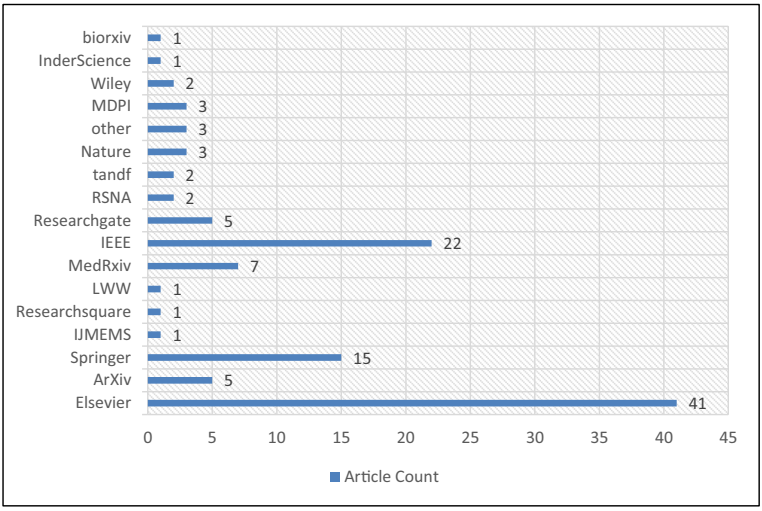

Fig. 2 Articles on Covid-19 diagnosis using DML

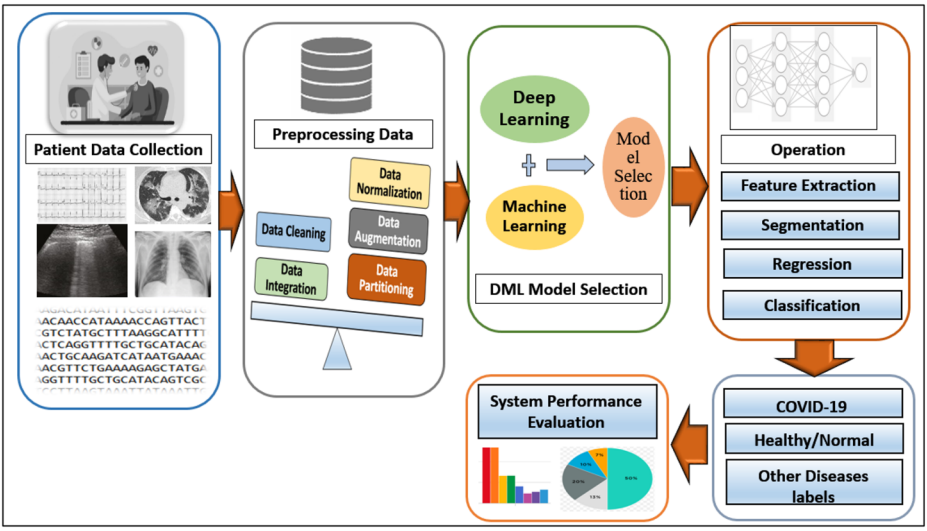

Fig. 3 Overall flowchart for Covid-19 diagnosis using DML

classification, which is then supported using the val dataset. The effectiveness of the produced model-feature space is assessed by employing a test dataset. Typical deep CNN architecture consists of a convo-layer, subsampling/down sampling/pooling layers(PL), and a fully connected(FC) layer. The convo-layer uses convolution action 'x' (multiply), a set of learnable filters called kernels that act as parameters. The prime objective of the convo-layer is to isolate the feature structure formed in the given input image of the local region. That is public data throughout the data sets, represented by a feature-structure map. The results of every convo-layer are served towards activation function to familiarize intermittence. The most popular activation function in DL is ReLU. The PL is optional and responsible for decreasing the multi-dimensional shape of input and resulting in reduced hyper-parameter from the network [109]. A PL gains every feature-structure map outcome from the convo-layer, and downsamples, i.e., the pool region reviews an area of neurons in the convo-layer. The famous pool is max-pool; it yields the highest rate in the input area. Each neuron of the FC layer is responsible for the previous layer coupled to the next layer of all neurons. Each significant weight and bias shows how powerfully a value equals a specific label-class [24]. The result of the last FC layer is directed to the activation function, which brings the outputs of the class totals to the highest value as a result. Finally, the recommended technique is assessed using performance metrics(-Section 8.2.1) such as accuracy, F1-score, specificity, precision, recall, etc.

Figure 4 shows the studied paper's analysis by the number of CNN architectures adopted to sense Covid19. The statistical analysis indicates that among all pre-trained DL models, mostly 34 reviewed systems used ResNet, and 24 systems used VGG. Because of various versions of ResNet including ResNet18, ResNet34, ResNet50, ResNet101, ResNet110, ResNet152/V2, ResNet164, ResNet1202 etc. ResNet makes utilization of residual blocks to increase classifier efficiency. The cornerstone of ResNet is the idea of "skip connections," which is root of residual blocks. Figure 5 shows the various DML tools and libraries used in the experimentation part for the automated recognition of Covid19. The more popular tools for automated Covid19 determination are Keras and TensorFlow because of their easy implementation and the accessibility of pre-trained models in these libraries.

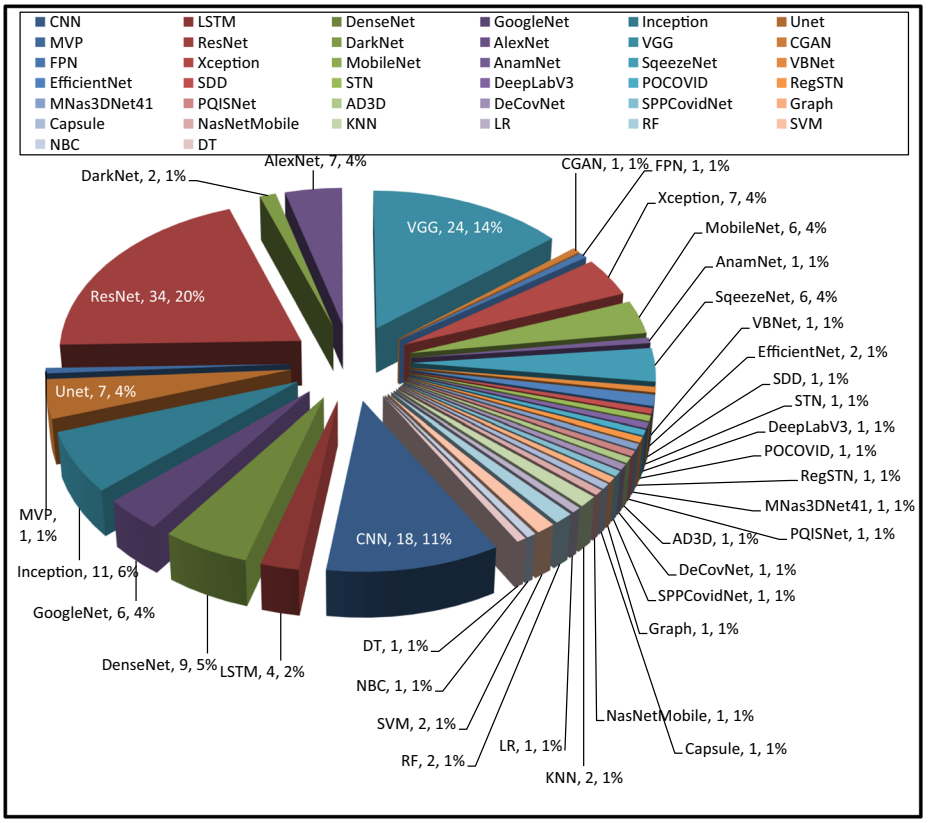

Fig. 4 DML models used in the studied papers for the diagnosis of Covid-19

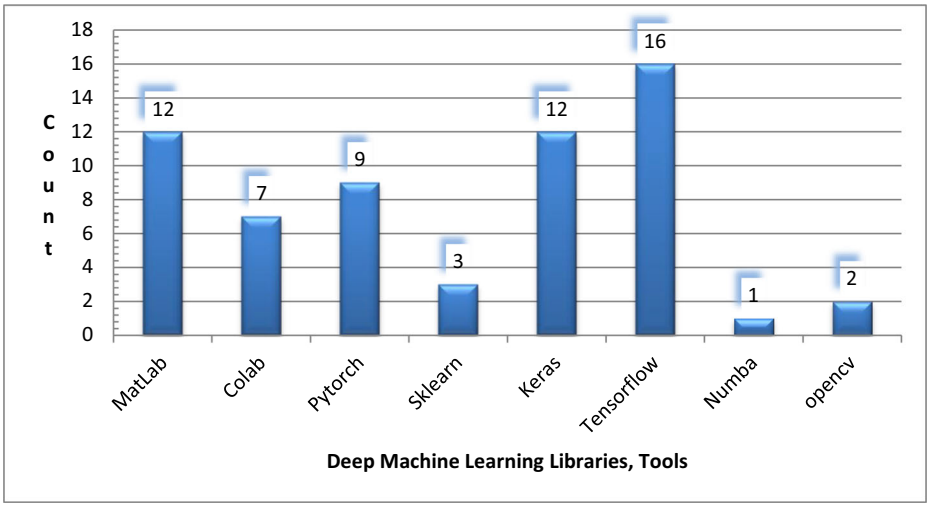

Fig. 5 Libraries / tools used for Covid-19 detection

2.2 Taxonomy of deep machine learning-based class wise task formulation and image modalities

Using radiography(X-ray, CT, ultrasound, ECG) images and genome sequence, DML approaches for classification have been used to construct several computer-aided diagnosis(CAD) systems. The major goal of classification systems is to recognize Covid-19 cases, which entails feature extraction, prioritizing the features, and classifying with deep layers. DML frameworks are employed to generate network structure that help in diagnosis of multi-class(Covid19, healthy, bacterial pneumonia, viral pneumonia) [75, 107, 131] or multi-class(Covid19, healthy, SARS1, SARS2) [46], 3-class(Covid19, healthy, pneumonia) [110, 122] and 2-class/binary(nonCovid, Covid19) [66, 70, 167]. Every disease label represents one or more classification categories.

Figure 6a shows the taxonomy distribution of the five categories of radiography images and genome sequencing from recently developed systems, and Fig. 6b shows the distribution of pre-trained and custom models. Taxonomy for categorizing the Covid19 detection method is offered throughout current work to aid field map-reading. We have selected taxonomy on the three multiple views of radiography modalities (X-ray, CT, and ultrasound) and other(ECG, genome sequence) used; each modality is linked to two DL methodologies (pre-trained and custom system). 2 categories of DL approaches are compared, such as pre-trained models with DTL and custom DL techniques. Furthermore, every DL-based diagnostic process is classified into X-ray, CT, ultrasound, ECG, and genome sequencing modalities. Throughout this study, we looked at 62 Covid19 detection systems. Using a broader point of perception, 32 examined methods (52% of the entire studied methods) deployed X-ray modality as a data source, while the 19 examined methods(31% of the total reviewed systems) applied on CT scans, 2 systems of ECG(3%), 2 systems of genome sequencing(3%) while the rest 7 systems (11% of the total studied systems) applied on ultrasound as shown in Fig. 6a. For Covid19 detection, 45 techniques (73% of the entire studied methods) employed pre-trained models, and 17 techniques (27% of the entire studied methods) were utilized by custom DL models, as shown in Fig. 6b.

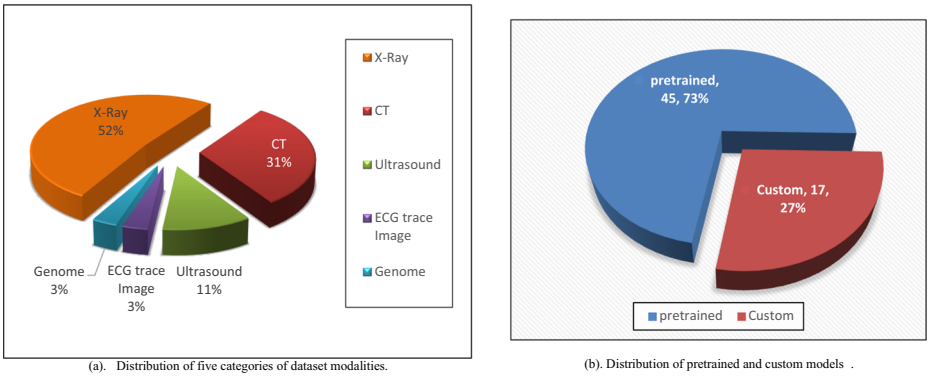

(a). Distribution of five categories of dataset modalities.

(b). Distribution of pretrained and custom models .

Fig. 6 Taxonomy used for DML-based Covid19 diagnosis from recently developed systems

2.3 COVID-19 dataset collection

From the reviewed papers, a total of 35 different datasets were retrieved. A summary of X-ray, CT, LUS, ECG, and genome sequence datasets is presented in Table 1. Several authors worked extremely hard and succeeded in creating a new clean Covid19 dataset [26, 62, 132, 142] from various medical institutes and research facilities and distributed it on public online platforms to open the community (Kaggle, Github, SIRM, Mendeley, Biorxiv, Medrxiv, NBAI Cancer imaging archive, Radiopedia, figure1, Medicalsegmentation, Zenodo, IEEE-Dataport, NIH, Wiki-Cancerimagingarchive). On the other hand, To comply with patients, health centre, and scientific laboratory privacy laws, the other researchers chose not to publish the database. Still, they did use the dataset for experiments purpose only [10, 82, 115, 136, 165, 167]. The dataset, resolution, mode, type, sampels/label, URLs, dataset location, and which researcher have used the set of data. These results indicate that the most popular dataset was from Cohen [54] Covid19 X-ray sample. The COVID19 multimodal data samples are shown in Fig. 7.

3 COVID-19 classification using X-ray images

3.1 Real-world pre-trained deep learning methodologies, evaluations with recent schemes

Islam et al. [72], in 2020, developed a Covid19 diagnosis system using a combined CNN and LSTM network. CNN was utilized for feature extraction, while LSTM was used to classify Covid19 on extracted features. The system considered 4575 X-ray samples from the multi-source public dataset [33, 36, 37, 83, 116, 157] with 3 classes. Where 1525 images of Covid19, 1525 images of normal, and 1525 images of pneumonia individuals. Samples were rescaled to 224 × 224 pixels. The composed data set was divided into 2-sets, i.e., train and test, in 80%(3660) and 20%(915), respectively. Accuracy and loss were attained by using 5-fold cross-validation. The suggested experimentation gained accuracy, specificity, sensitivity, and F1-score of 99.2%, 99.2%, 99.3%, and 98.9%, respectively. Bassi et al. [13], in 2021, suggested an innovative accumulation to the twofold transfer learning method, i.e., the network would be first trained on ImageNet with five DNNs, named NetworkA, NetworkB, NetworkC, NetworkD, and NetworkE. Network A, B, and C structure has 201 layers of DenseNet, and Network D, E has 121-layer of DenseNet with added arbitrary weights and biases. The dataset was randomly partitioned with 80% of the samples for the training and validation set of 20%. The dataset [116] was divided into three classes (normal, pneumonia, Covid19). For the test set, 50 random images were chosen among every class (normal, pneumonia, Covid19). After eliminating 150 test samples, 90% of the remaining samples casted for training and 10% for validating. The experimental results on the proposed system achieve the highest accuracy by DNN C Network with 100%, whereas A Networks achieve 99.3%, and B Network reaches 98.7%. Jain et al. [75], in Oct. 2020, proposed a DTL scheme with a two-stage strategy, i.e., data augmentation, and preprocessing in stage-1 and stage-2 contains designing the deep network model. The assembled 1215 X-ray images from Github [83] and Kaggle [54] datasets. Further data augmentation strategy raises the sample size to 1832 and trains the network on pre-trained ResNet50, ResNet-101, and ImageNet networks. The scheme used a 5-fold cross-validation process. The first stage model distinguishes between viral pneumonia, bacterial pneumonia, and healthy, and the second phase network

Table 1 Covid-19 Dataset [18] and repositories used in the studied research papers

Dataset	Used in COVID19 Articles	Data Source Name	Resolution	Mode	Type	Images	URL
[33]	[49, 72]	Github: Agchung.	224×224	X-ray, CT	JPG	55 (Covid19) CT, Xray.	1)github.com/agchung/Figure1-COVID-chestxray-dataset/tree/master/images. 2)github.com/agchung/Actualmed-COVID-chestxray-dataset.
[36]	[49, 72, 81, 86, 126]	RICORD data set (Open survey by the RSNA).	Variable Sizes	X-ray, CT	DICOM	1000 Chest Xray, 240 thoracic CT exams.	1)radiopaedia.org/articles/imaging-data-sets-artificial-intelligence. 2)radiopaedia.org/articles/Covid-19-4?lang=gb#article-images.
[157]	[17, 72]	Covid19 AR.	1024×1024	X-ray	DICOM	105 Subjects of Covid19 AR.	nbia.cancerimagingarchive.net/nbia-search/.
[37]	[1, 7, 12, 15, 40, 47, 58, 59]	SIRM-Covid19 Database.	Variable Sizes	X-ray	JPG	115(Covid19)	sirm.org/category/Covid-19/. www.sirm.org/category/senza-categoria/Covid-19/.
[54]	[2, 12, 21, 46, 49, 70, 75, 81, 82, 85, 86, 90, 101, 107, 110–112, 118, 121, 122, 125, 126, 130, 143, 144, 158, 170]	Github: Covid Chestxray-Dataset (Cohen).	Variable Sizes	X-ray, CT	JPG, PNG	930(Covid19), MERS, SARS.	github.com/ieee8023/covid-chestxray-dataset.
[83]	[2, 19, 21, 72, 75, 81, 82, 86, 90, 111, 118, 121, 126, 144, 170]	Kaggle: Chest Pneumonia X-ray Images.	Variable Sizes	X-ray	JPG	5856(Pneumonia)	www.kaggle.com/paultimothymooney/chest-xray-pneumonia.
[116]	[13, 19, 21, 64, 72, 111, 112]	NIH Chest X-rays (ChestX--ray14 pulmonary disease, ChestX-ray8).	Variable Sizes	X-ray	PNG	112,000(Other than Covid diseases), Summers, Ronald (NIH/CC/DRD), Enterprise Owner NIHC Center.	www.kaggle.com/nihchestxrays/data?select=Data_Entry_2017.csv.nihcc.app.box.com/v/ChestXray-NIHCC.

Table 1 (continued)

Dataset	Used in COVID19 Articles	Data Source Name	Resolution	Mode	Type	Images	URL
Private	[165]	Xi'an Jiaotong Univ., Nanchang Univ., Hospital of Xi'an Medical College.	395×223, 636×533	CT		1065(Covid19)	Private Dataset
[56]	[77, 93, 150, 171]	SARSCOV2 CT-Scan Dataset- Brazil. (Hospital Sao Paulo).	Variable Sizes	CT	PNG	1252(Covid19), 1230 CT-samples of non-Covid patients.	www.kaggle.com/plameneduardo/sarscov2-ctscan-dataset.
Private	[82]	3 Hospitals in India and other nine-country.	Variable Sizes	X-ray	DICOM	659(Covid19), 1660(Healthy), 300(Abnormal), 4265(NonCovid).	Private Dataset
[40]	[64, 85, 98, 142]	Covid-CT: CT dataset Covid19 (Xingyi Yang).	Variable Sizes	CT	JPG	349(CT images, clinical findings of Covid19 216 patients).	github.com/UCSD-AI4H/COVID-CT.
[25]	[63, 98]	Biorxiv Dataset.		CT			www.biorxiv.org/
[104]	[63, 98]	Medrxiv Dataset.		CT			www.medrxiv.org/
[48]	[49, 126]	figure1 Covid19 clinical cases.	Variable Sizes	X-ray	PNG	35(Covid19(	www.figure1.com/Covid-19-clinical-cases
[38]	[2, 21, 49, 70, 118, 148, 158]	Kaggle: Covid19 Radio Database: X-ray (M.E.H.Chowdhary)	Variable Sizes	X-ray	PNG	3616(Covid19)	www.kaggle.com/tawsifurrahman/covid19-radiography-database
[129]	[49, 131, 143, 170]	Radiological Society of North America.	Variable Sizes	X-ray	DICOM	9555(Pneumonia), RSNA pneumonia.	www.kaggle.com/c/rsna-pneumonia-detection-challenge/
[114]	[132]	Negin medical center, Sari(Iran).	512×512	CT	DICOM	15,589 Covid19 lung HRCT images.	github.com/mr7495/COVID-Ctset
[35]	[124]	Covid19 Segmentation Data.	Variable Sizes	CT	JPG	100(Covid19 Samples)	http://medicalsegmentation.com/covid19/
[55]	[112, 122]	Github: Muhammedtalo X-ray.	Variable Sizes	X-ray	JPG	125(Covid19, No Finding, Pneumonia).	github.com/muhammedtalo/Covid-19/tree/master/X-Ray%20Image%20DataSet
[34]	[93]		Variable Sizes	CT	JPG		

Table 1 (continued)

Dataset	Used in COVID19 Articles	Data Source Name	Resolution	Mode	Type	Images	URL
		Covid19 CT Lung, Infection Segment Dataset.				20(Labeled Covid19 CT scans).	zenodo.org/record/3757476#.YNBXMt3hXIU
[67]	[93]	IEEEDataport: CCAP-CT data sets from multi-Centre hospitals.	Variable Sizes	CT	JPG	42(chest CT scans of Covid19).	ieee-dataport.org/documents/ccap
[39]	[101, 107, 125]	Kaggle Covid19 Xrays, CT snapshots.	Variable Sizes	X-ray, CT	JPEG	79(Xray), 16(CT Covid19).	www.kaggle.com/andrewmvd/convid19-x-rays
[84]	[103]	Kaggle Covid19 Chest X-ray: Covid19 image data collection (Bachrr).	Variable Sizes	X-ray	JPEG	357(Covid19).	www.kaggle.com/bachrr/covid-chest-xray
[52]	[17, 62]	Github Arthursdays HKBU-HPML-Covid19 CT dataset (Clean-CC--CCII).	Variable Sizes	CT	JPEG	340,190(CT Slices of Covid19).	github.com/arthursdays/HKBU_HPML_Covid-19
[89]	[107]	Daniel Kermany et al.: Large Dataset of Labeled OCT and X-ray	Variable Sizes	X-ray, CT		CNV, DME, Drusen, and Normal (ZhangLabData).	data.mendeley.com/datasets/rscbjbr9sj/3
[28]	[17, 27, 64, 108]	POCOVID-Net Data set (POCUS)	Sliced images from UT videos	Ultra-sound	More than 200 LUS videos (Convex, Linear)	Images:22(Covid19), 22(Bacterial Pneumonia, 15(Healthy), Viral Pneumonia. Videos:115(Covid19), 51(Bacterial Pneumonia), 75(healthy), 6(Viral Pneumonia).	github.com/jannisborn/covid19_ultrasound/tree/master/data
[30]	[144]	Indiana University Hospital.	Variable Sizes	X-ray	DICOM, PNG	Chest X-ray images.	openi.nlm.nih.gov/
[5]	[158]	A. Ahmed GitHub: Pneumonia.	Variable Sizes	X-ray	JPEG	163(Pneumonia).	www.kaggle.com/ahmedali2019/pneumonia-sample-xrays
[74]	[139]		Variable Sizes	Ultra-sound	Video		iclus-web.bluetensor.ai.

Table 1 (continued)

Dataset	Used in COVID19 Articles	Data Source Name	Resolution	Mode	Type	Images	URL
		Italian Covid19 Lung Ultrasound DataBase(ICLUS-DB).				277-LUS Videos(58,924 frames)	
[53]	[26]	Github: BorgwardtLab.	Variable Sizes	Ultra-sound	202 videos	Bacterial, Pneumonia, NonCovid, ViralPneumonia, Healthy, Covid19.	github.com/BorgwardtLab/covid19_ultrasound.
[42]	[21]	Pulmonary X-Ray Abnormalities.	Variable Sizes	X-ray	PNG	336(tuberculosis), 326(normal).	www.kaggle.com/kmader/pulmonary-chest-xray-abnormalities
[149]	[19]	SIIM-FISABIO-RSNA.	Variable Sizes	X-ray	DICOM	7600(COVID19 xray samples).	www.kaggle.com/c/siim-covid19-detection
[91]	[20]	Paper-based ECG-trace image.	Variable Size	ECG	JPEG	250(COVID19), 77(MyocardialInfarction), 548(Abnormal heart beats, 203(History of MI), 859(Normal).	data.mendeley.com/datasets/gwbz3fsgp8/1 or doi.org/10.17632/gwbz3fsgp8.1
[123]	[61]	PACIFIC-RNA SEQUENCE.	Variable Genome Sequence length.	Genome Sequence	.fa and .txt file	SARSCoV2, Influenza, Metapneumovirus, Rhinovirus, Coronaviridae.	github.com/pacific-2020/pacific/ Or doi.org/10.1038/s41598-021-82043-4
[1]	[61]	RCoV19(GISAID+GenBank+CNGBdb+NMDC RCoV19).	Variable Genome Sequence length.	Genome Sequence	.fa and .txt file	1337 SARSCoV2 sequences.	https://doi.org/10.16288/j.yczz.20-030 Or bigd.big.ac.cn/ncov

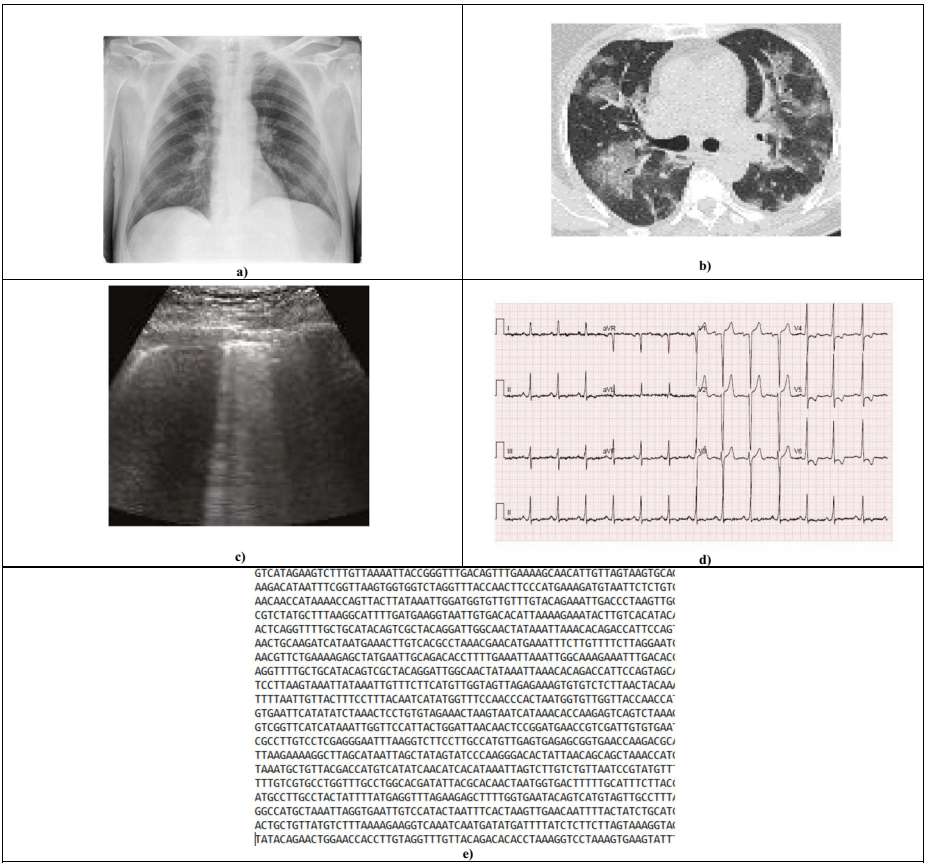

Fig. 7 COVID19 multimodal dataset samples. **a**) X-Ray [37], **b**) CT [129], **c**) Ultrasound [28], **d**) ECG [51], **e**) Genome Sequence [91]

detects the occurrence of Covid19. The simulation outcomes achieved accuracy, recall, and precision of 97.77%, 97.14%, and 97.14%, respectively. Ozcan [121], in May 2020, proposed a DL structure for corona virus disease classification from X-ray using a grid search(GS) and pretrained assisted DNN model. Classical DL variants (GoogleNet,ResNet18,ResNet50) were used for categorization, feature mining, transfer learning purposes, and selecting the best hyper-parameter with the GS technique. Ozcan assembled 721 images from 3 public multi-source datasets [37, 54, 83], where the images of 242 for bacteria, 200 for normal, 148 for viral, and 131 for Covid19 classes. The assembled dataset was partitioned to 50:30:20 ratios in the proportion of train, test, and validation sets, respectively. After experimentation on the X-ray dataset with four classes, the projected method has achieved the best results for the GS ResNet50 technique with an 97.69% accuracy, 95.95% precision, 97.26% sensitivity, and 97.90% specificity, and 96.60% F1-measure.

Additionally, Joshi et al. [82], Jan. 2021, proposed a robust DTL adopted Covid19 sorting structure from X-ray. Covid19 positive X-ray images from various nations, including three hospitals in India, Australia, and 12 other countries, were chosen for training model performance assessment. The pre-trained DarkNet53 was used for feature extraction and generated a

feature pyramid network with ImageNet. Assembled multisource CXR dataset contains 659 instances of Covid19, 1660 images of healthy, and 4265 images of nonCovid. The dataset was divided into training, 5-fold cross-validation, and test. They attained test accuracy of 97.11% for ternary-class(Covid19, normal, pneumonia) and 99.81% for binary(Covid19, nonCovid) classification with disease detection 0.137 s per image. Furthermore, Fontanellaz et al. [49] proposed a completely automated study in June 2021 that employs depth-wise with an inverted convolution block for feature extraction on a prognostic structure to find X-ray-based Covid19 pneumonia. The inverted bottleneck chunks were utilized to construct down sample and feature maps. The combined and down sampled feature maps were fed to an MLP, which delivers the model produced in the form of a likely possibility for the healthy, other-pneumonia, and Covid19-pneumonia class. They employed multisource publically available online datasets [33, 38, 54, 129] containing normal X-ray, Covid19-pneumonia confirmed, and other-pneumonia classes. After synchronization of the dataset, the training set comprised 7966(normal), 5451(other-pneumonia), and 258(Covid19-pneumonia) classes. However, 100 samples were assigned to each class in the test set. The projected system attained overall diagnostic accuracy of 94.3%, the sensitivity for normal CXR, other-pneumonia, and Covid19-pneumonia 98.0%, 88.0%, 97.0% respectively, PPV of 94.5%, F1-score of 94.3%. After merging other pneumonia and Covid19-pneumonia cases, the projected network acquired an accuracy of 95.7%. Moreover, Irmak [70], in Nov. 2020, designed a robust CNN model and planned to detect Covid19 using publicly available multisource datasets. Assembled datasets from two online public platforms [38, 54] were categorized into 625 for Covid19 and 625 for nonCovid19 classes. This experimented model is adopted to resolve whether a specified CXR image has Covid19 or not with an 99.20% accuracy, 98.41% specificity, 100% sensitivity, 98.41% precision, and AUC of 99.98%.

Rafi [130], in Oct. 2020, used two pretrained models(ResNet152, DenseNet121) to identify Covid19. The obtained dataset was sliced into 70%:30%(training:testing) for binary classification(Covid19 and normal). The proposed experimented ensemble (ResNet152 + DenseNet121) model achieves the highest results with an 98.43% accuracy, 99.23% specificity, and 98.71% sensitivity. Panwar et al. [126], in Sept. 2020, developed an algorithm using DNN based method called “nCOVnet” to identify Covid19 using Xrays. They employed datasets from three public platforms [36, 48, 54] containing 142 instances of Covid19 positive and 142(healthy patients), and 5863(pneumonia). Xray samples were sliced into healthy, bacterial-pneumonia, and viralPneumonia with different class values. The assembled dataset was separated into 70% for training(127 patients) and 30% for testing (31 cases) set. Because of the small sample size and the lack of a pixel ratio, they transformed all images to 224 × 224 pixels and used the data augmentation technique with a rotation range of 20 degrees. The experimental results correctly sense the Covid19 positive individuals with an 97% accuracy, whereas 88% inclusive accurateness, 97.62% sensitivity, and the specificity of 78.57%. Nayak et al. [112], in Feb. 2021, used eight variants of CNN (VGG16, ResNet34, MobileNetV2, AlexNet, SqueezeNet, and InceptionV3) for the prediction of Covid19 from CXR. Nayak composed multisource data from 3 public platforms [54, 55, 116]. The data collection was divided into 70%:30% for training, testing. A sum of 286 frontal-view CXR samples were considered, comprising 143(Covid19) and 143(healthy) class in the training and 120(Covid19), and 60(healthy) class in the test set. However, the selected dataset was small; later data augmentation was used to increase the number of instances. In terms of model results, ResNet outperformed the competitive edge. Compared with other networks, the best

results were attained by ResNet34 with an accuracy, AUC, precision, specificity, and F1-score of 98.33%, 98.36%, 96.77%, 96.67%, and 98.36%, respectively.

Furthermore, Das et al. [110] in Jul. 2020, created an autonomous Covid19 finding technique with DTL based on Inception (Xception) from CXR. They collected a single-source dataset [54] and divided it into 70%(training), 20%(testing), and 10%(validation) ratios. Covid19(+), pneumonia(+), and Covid19(−) were used as classifications in this investigation. The system achieved a performance of training analysis with 99.52% accuracy, 98.62% F-measure, 99.12% sensitivity, 99.46% specificity, 98.08% kappa stats, and testing analysis with 97.40% accuracy, 96.96% F-measure, 97.09% sensitivity, 97.29% specificity, 97.19% kappa stats respectively. Ozturk et al. [122], in June 2020, projected a novel model (DarkNet) for automatic recognition of Covid19 using raw CXRIs. The Darknet model was trained on 127 CXRI of the dataset repository [54, 55]. The assembled multisource dataset contains 1125 images for training the proposed model, including 125 frames for the Covid19(+) class, 500 frames for the pneumonia class, and 500 frames for the no-findings class. The experiment achieved 98.08% binary classification accuracy(Covid, no-findings) and 87.02% for 3-class(Covid, no-findings, pneumonia) classification and 95.13% average sensitivity, 95.30% specificity, and 96.51% F1score. Narin et al. [111], in May 2021, suggested automaed discovery of COVID illness detection using CXR radiographs. They employed 5 pre-trained CNN variants (InceptionV3, InceptionResNetV2, ResNet50, ResNet101, and ResNet152). This study fulfilled three altered binary classifications with 4-lables, i.e., Covid19, normal, viralPneumonia, and bacterialPneumonia via 5-fold cross-validation. From 3-datasets [54, 83, 116], accuracy with 96.1%(Dataset1), 99.5%(Dataset2) and 99.7%(Dataset3) attained by pre-trained ResNet50.

In an alternative study, Pandit et al. [125], in May 2021, suggested the spontaneous discovery of Covid19 from CXR using the pretrained VGG16 model. The projected model uses a non-connection procedure to define if the radiography image is diseased. In this work, 2-public datasets [39, 54] were used, containing 1428 images with 224 for Covid19 confirmed positive class, 700 for communal bacteria pneumonia class, and 504 for healthy class with no infection. Randomly dividing the dataset into training and test sets, with 70% belonging to training and 30% to the testing set. Experiment achieved accuracy of 96% and 92.5%, sensitivity(TPR) of 92.64% and 86.7%, specificity(TNR) of 97.27% and 95.1% in binary(Covid and nonCovid) and 3-class(Covid, nonCovidPneumonia, and healthy) cases, respectively. Later, Medhi et al. [103], in May 2020, developed spontaneous recognition of Covid19 contamination from CXR using the DL multilayer CNN. The publicly available dataset from Kaggle [84] has been used in this study contains 150 confirmed Covid19 patients. A patchy white shadow over the lung region led to the diagnosis of Covid19 infection. The proposed system has data acquisition, pre-processing (noise removal using 2D Gaussian filter), segmentation (gray level threshold), extracting the features using multilayer CNN structure, and classification (softmax activation function) steps. The experimented system shows the projected system's outcomes that recognize the Covid19 cases with 93% accuracy. Abbas et al. [46], in May 2020, proposed the classification of Covid19 from CXR using DeTraC (Decompose-Transfer-Compose) DCNN. To prove the strength of DeTraC, it internally uses 5 variants of CNN(ResNet, GoogleNet, AlexNet, VGG19, and SqueezeNet) in the transfer learning stage. The AlexNet pretrained network centered on a shallow learning approach to mine discriminative features of the 3-classes (normal, Covid19, SARS) for the class

decomposition layer. The decompose class aims at improving small discrepancy classifiers assisting additional flexibility to their decision boundaries. The authors collected the data source from multisource public platforms [54], and 2 datasets from JSRT contain high-resolution images, i.e., 4020 × 4892 and 4248 × 3480 pixels. The PCA technique was used to plan the high-aspect feature space with a target on a lower dimension to deal with high-resolution images. The dataset was sliced into 70:30 ratios for training:validation set into norm1 class with 441 images, norm2 class with 279 images, Covid19–1 class with 666, Covid19–2 class with 283, SARS1 class with 63, and SARS2 class with 36 images. The performance of DeTraC was compared with pre-trained models for both shallow and deep tuning modes. DeTraC, through VGG19, has succeeded with the uppermost 97.35% accuracy, 98.23% sensitivity, and 96.34% specificity.

3.2 Real-world hybrid & custom deep learning methodologies, evaluations with recent schemes

Abdani et al. [2] in Jul. 2020 suggested a lightweight DL model by implanting an altered spatial pyramid pooling (SPP) module into the CNN to monitor the possibility of Covid19. The 4-open-source databases [37, 38, 54, 83] containing 219(Covid19 positive), 1341(normal), and 1345 images of viral pneumonia class. The suggested method is called SPP-COVID-Net and has a sum of 862,331 parameters. The base of the SPPCOVIDNet network is imitative from DarkCovid-Net. In DarkCovid-Net, a multi-scale approach was implanted by exchanging the last few layers of the new structure with parallel PLs of SPP. The system classifies an CXRIs into 3-classes(Covid19,healthy and other types of viral-pneumonia). The experimental setup for SPPNet achieve 94.6% accuracy. Rahimzadeh et al. [131], in 2020, introduced a new DL model based on hybrid networks of Xception and ResNet50V2. Based on [129] open-source dataset, the system trained a hybrid structure for distinguishing CXRIs into 3-classes(healthy, pneumonia, Covid19). The merged network is created by combining the extracted features of Xception and ResNet50V2 and then feeding the integrated extracted features to the convo-layer of the classifier. According to experimental findings, the suggested network's average accuracy for identifying Covid19 instances was 99.56%, while the overall accuracy for altogether classes is 91.4%.

Nour et al. [118], in Dec. 2020, offered a Covid19 intelligence diagnostic model based on CNNs. The suggested model ensures end-to-end learning and is trained from the start (contrary to transfer learning), with weights of 9 × 9 × 3 × 128, bias 1 × 1 × 128 that may directly learn extracted features from the input X-ray samples. This CNN model was used for feature extraction. Deep features were served in ML techniques for the decision tree, SVM, and KNN. The Bayesian optimization technique was utilized to maximize the ML model hyperparameter. The experimentations were carried out on images from an open Covid19 database [38, 54, 83], with original images of 219(Covid19), 134(healthy), and 1345(viral pneumonia) classes. Later data augmentation was applied to increase the sample size of the data set. The SVM classifier offers the highest 98.97% accuracy, 89.39% sensitivity, 99.75% specificity, and 96.72% F1-measure.

A recent study by Aslan et al. [12] in Jan. 2021 proposed hybrid architecture (mAlexNet+ BiLSTM). Two learning algorithms were suggested for accurately identifying positive Covid19 patients using CT and CXRIs. As part of preprocessing, the lung segmentation in CT scans to obtain robust features was given as input to these suggested designs, and it was achieved spontaneously using ANN. Both structures comprise AlexNet for transfer learning.

The second suggested structure was a hybrid arrangement containing a BiLSTM layer. The system considered 2905 samples, including Covid19(219), Viral-Pneumonia(1345), and Normal(1341) cases. ANN-based lung segmentation results in image conversion to 1024 × 1024 pixels. With data augmentation to the Covid class, the samples increased to 1095. The input image fed to mAlexnet requires the image input layer 227 × 227 × 3 images with each convolayer followed by ReLU. The final FC8 layer weights are fed to BiLSTM. BiLSTM uses RNN to process sequential data. The CNN and BiLSTM network time for training was 139 and 85 seconds. The training time for the mAlexnet structure took 139 seconds. Whereas training hybrid structure took 224(139 + 85) seconds. The simulation results of the suggested system for the first mAlexNet Covid19 recognition rate of 98.14% accuracy, 98.26% recall, 99.06% specificity, 98.16% precision, 98.20% F1-score. The second result by, mAlexNet+BiLSTM hybrid architecture with 98.70% accuracy, 98.76% recall, 99.33% specificity, 98.77% precision, and 98.76% F1measure.

4 COVID-19 classification using computed tomography (CT) images

4.1 Real-world pre-trained deep learning methodologies, evaluations with recent schemes

Wang et al. [165] reported a method to sense Covid19 in CT scans using the concept of pretrained models in 2021. The suggested method took advantage of two prominent pretrained models (GoogleNet, InceptionV3). The combined dataset consisted of CT scans from 3 different universities and hospitals consisting of 1065 Covid19 images. The proposed neural network system was divided into 2-parts: in the first portion, the pretrained Inception was used to transform samples to 1-D vectors. The second portion is a FC network primarily used for classification. Parameters were trained for 1500 epochs, with the initial learning rate of the pretrained model being 0.01. The experimental setup reveals that the network attained accuracy, AUC, specificity, sensitivity, and F1-measure of 89.5%, 95%, 88%, 87%, and 77%. Ni et al. [115], in Dec. 2020, proposed a DL algorithm for illness detection, classification, and positive pathogen determination. They compiled private datasets from three hospitals in China containing approved 14,435 chest CT images. MVP-Net and 3DUnet were used in the proposed network. The procedure was assessed in a non-duplicated datasource of 96 affirmed Covid19 individuals. The results obtained were compared with three radiological inhabitants and two experienced radiologists. The experimented results achieve precision, AUC, affectability, specificity, and F1-score of 93%, 86%, 97%, 97%, and 94%, respectively.

Using DL, Xu et al. [167], in Oct. 2020, created the Covid19 diagnostic system. For feature extraction, ResNet-18 with a location-attention network structure was employed. A pooling method was also utilized to reduce dimensionality and prevent overfitting. They compiled private datasets from four Chinese hospitals and universities. The sum of CT scans in the compiled dataset is 618, with samples of 219 for Covid19, 224 for IAVP, and 175 for healthy classes. A model discovery comprises image classification to detect the appearance and structure of distinct illnesses. The radius out from the edge was utilized to identify Covid19, an additional weight for the algorithm, to acquire the relative position of the patched on the pulmonary scan. The experimental result brings an 86.7% accuracy, 81.3% precision, and 83.9% F1-score. Loey et al. [98], in Oct. 2020, used the data augmentation technique with the conditional generative adversarial network (CGAN) with DTL to detect the corona virus. It

employs 5-distinct (AlexNet, VGG16,VGG19, GoogleNet, ResNet50) pre-trained DCNN models. The reason for adopting CGAN is that the amount of Covid19 samples was limited; thus, they added data augmentation with CGAN for expanding the samples size with improved accuracy. The dataset was compiled from three online public platforms [25, 40, 104], with 742 samples divided into four label classes for experimentation (Covid19, Augmented-Covid19, CGANCovid19, and AugCGANCovid19). According to the experimental results based on different class levels, a high balanced ResNet has a 82.64% testing accuracy, 88.30% sensitivity, and 93.33% specificity. In comparison, VGGNet19 has a testing accuracy of 76.54%.

Saeedi et al. [142], in Oct. 2020, introduced a CAD web-service to detect Covid19. The suggested web-based DNN hybrid architecture uses ResNet, Inception, and MobileNet. A single public dataset [40] was used for the experiment. 746 samples were selected, including Covid19(349) and healthy(397) class. The suggested approach uses nuSVM, which acts as anti overfitting bottleneck. The operation includes reducing image dimensions (to reduce parameters) and increasing system performance by utilizing the previous layer's outputs as inputs. Lastly, an amalgamation of DenseNet was used to classify Covid19 and healthy classes. The proposed experiment produced 90.61% accuracy, 90.80% recall, 89.76% precision, and 95.05% AUC. Cruz [63], in 2021, proposed the stacked ensemble method and binary phase TL to sense Covid19. The system used 6 variants of CNN (VGG16, ResNet50, ResNet50–2, DenseNet161, DenseNet169, and Inceptionv3). The network contains 128 neurons and ReLU activation classifier layers by replacing the last layers of VGG16. Dataset was assembled from multisource online public platforms [25, 104]. A sum of 746 CT scans was considered for the experiment among 349 for Covid19 and 397 for non-Covid. The results were obtained from binary classification. The experimented results achieved an 86.70% accuracy, 85.86% F1-measure of and 90.82% AUC.

Through High-Resolution Computed Tomography (HRCT) scans, Ardakani et al. [10] in Jun. 2020 suggested a method to identify Covid19 utilizing 10 CNN forms (ResNet18, ResNet501, ResNet101, VGG16, VGG19, AlexNet, SqueezeNet, GoogleNet, MobileNetV2, and Xception). They collected private datasets from 16 hospitals. For the simulation, a sum of 1020 CT pictures were considered, including Covid19(510 images) and non-Covid (510 images) individuals. The datasource were partitioned into 80:20% for training:validation sets. ResNet101 and Xception give better results than the other 10-networks. The Xception network achieved an 99.02% accuracy, 98.04% sensitivity, 87.3% AUC, and 100% specificity based on the experimental data. The ResNet101, on the other hand, attained 99.51% accuracy, 100% sensitivity, 99.4% AUC, 99.02% specificity, 99.27% PPV, and 100% NPV.

4.2 Real-world hybrid & custom deep learning methodologies, evaluations with recent schemes

In 2020, Rahimzadeh et al. [132] suggested a completely automated DL-based feature pyramid network (FPN) for the Covid19 prediction based on large CT samples. They introduced a novel dataset COVID-CT Set [114]. COVID-CT dataset comprises 48,260 healthy CT images and 15,589 images of Covid19 contamination. Custom-developed FPN automatically removes those CT samples that are not adequately visible or are impure. This benefit shrinks the number of samples needed for processing and false discovery. FPN aids the system in improved learning and sensing multiscale elements that may be present in an image. The experimental setup used a modified DCNN variant of ResNet50V2 and was improved by the FPN for categorizing the carefully chosen samples to Covid19 or normal classes.

ResNet50V2-FPN reached 98.49% accuracy with 7996 validation samples during the image classification phase. To identify Covid19, Wang et al. [164] in Aug. 2020 recommended a 3D-DCNN(DeCoVNet). Weakly supervised neural network architecture was developed for Covid19 identification using 3D CT scans. Using Unet, the segmentation of the chest section was pre-trained. The privately assembled CT datasets from various radiology departments (Union Hospital, Tongji Medical College, HUST) were considered for the experiment. For acquiring a CT lung mask, regions were segmented using unsupervised learning and manually discarded failed cases. Experimented results obtained an accuracy of 90.10%.

Han et al. [59], in Aug. 2020, proposed a custom AD3DMIL learning algorithm. Attention-based 3D multiple instances learning(AD3D-MIL) contains a container of instances where each patient marker was allotted to 3D CT lung images. The primary goal of AD3D-MIL was to compute a separate group label for CT. The primary responsibilities were classifying Covid19 as common pneumonia or no pneumonia and locating the infected lung area. AD3DMIL generates deep 3D cases like the possible infection area of Covid19, common pneumonia, without pneumonia. Further, AD3D-MIL relates the attention-based pooling method to 3D cases to deliver comprehension into the involvement of every case to the sack label. At last, for more accessible learning, AD3D-MIL learns Bernoulli distributions of the bag-level labels. A total of 460 chest CT scans collected privately were considered for the experiment, including 230 CT images for Covid19, 100 CT images for common pneumonia, and 130 CT images without pneumonia. Experiment results reveal that the AD3D-MIL algorithm achieves 97.9% inclusive accuracy, 99.0% AUC, and a kohen-kappa-score of 95.7%.

Moreover, Paluru et al. [124] in Mar. 2021 proposed a scheme for anamorphic depth (AD) implanting-based lightweight CNN to segment irregularities in Covid19 CT images. The projected AnamNet consumes 7.8 times lesser parameters equated to Unet. AnamNet becomes lighter as a result of this feature and capable of providing inference to resource constraint devices like mobile, IoT(Raspberry Pi) [21] platforms. AnamNet first extracts the lung region called a lung mask using U-net. Then extracted lung region was used for forecasting Covid19. The proposed experimented AnamNet offers 98.80% accuracy, 99.70% specificity, 91.10% sensitivity, and an overall 94.10% dice-score. Still, 95% accuracy in the normal lung region, and 68.00% in abnormal region**.** Konar et al. [93], in 2021, proposed a semi-supervised shallow learning network with an automatic diagnostic for Covid19 using pulmonary CT imaging. The suggested architecture incorporates a Parallel Quantum-Inspired Self-supervised network (PQIS-Net) without pretrained CNN models for automated segmentation of lung CT slices traveled over FC layers. The PQIS-Net model works parallel three-layer configurations consisting of interrelated quantum bits, the second-order n-connected neighborhood-based network for segmentation of lung CT images, and differences in local intensities. They have collected three publicly available datasets [34, 55, 56] for the experiment. The dataset [54] was used for segmentation, and the other two datasets were utilized to classify Covid19. The examined system achieved an 98.4% accuracy, 98.6% precision, 98.5% recall, 97.8% AUC, and 98.3% F1-score.

5 COVID-19 classification using ultrasound images

Ultrasound has historically been used for diagnoses in cardiovascular [88, 161] and maternity care, and more recently for a variety of new illnesses, including kidney disease detection [117], spondyloarthropathies [41], atherosclerosis [154], etc. Another cause would be that technology

improvements, particularly computer vision, have enabled the determination of important data using the poor level and the high signal-to-noise images of the ultrasound modality [64], which is increasingly used in ultrasound. Currently, several studies have employed ultrasound as just a useful diagnostic tool for hepatocellular carcinoma [95], endometriosis [169], and pseudo tumor cerebri [44]. The integration of pulmonary ultrasound utilizing DNN has been proven beneficial for evaluating lung ultrasonography quicker and easier at the bedside with respiratory failure. Covid19 detection using DL-based lung ultrasound (LUS) needs to perform essential tasks like frame-based sorting, video-based scale classifying, and pathological artifact segmentation.

LUS imaging is an instrumental technique when the patient flow limit exceeds the clinic radiology set-up competencies due to its wide range of applicability and relatively affordable budget. Because of the low fees, it is also accessible to lower-economic countries. However, in addition to X-ray, CT radiology DL-based image processing, LUS datasets are accessible in the form of images/frames and videos for training. If a dataset is of the video type, converting it to a frames dataset requires additional computation. In addition, the time-series procedure adds further preprocessing to the LUS dataset.

5.1 Real-world pre-trained deep learning methodologies, evaluations with recent schemes

In August 2020, Roy et al. [139] developed a novel deep network(imitative of STN) that calculates the infection strictness mark connected to an input frame and provides the weakly monitored location of infected items. Roy developed a new technique based on uni-norms for in-effect aggregation of frame scores on the video level. Finally, the standard deep model was created to evaluate pixel-level segmentation of the Covid19 ultrasound image. The ultrasound dataset was collected from Italian hospitals(ICLUS-DB) [74] for experiment purposes. The employed dataset contains annotations on 4-level scales on frame, and video-based. It also comprises a subsection of pixel-level tagged LUS frames. The proposed model named Reg-STN uses CNN, STN, Unet, Unet++, and Deeplabv3+ as the backbone. Acquired a total of 58,924 frames corresponding to 277 videos, comprising 45,560 frames using convex probes and 13,364 frames using linear probes, which were labeled based on the scoring criterai (score range of 0 to 3). The labeled frames dataset consists of 19,973 frames for score-0(34%), 14,295 frames for score-1 (24%), 18,972 frames for score-2 (32%), and 5684 frames for score-3 (10%). Also, 60 videos sample was selected for video-level annotations. A total of 1005 convex probes and 426 linear probes frames acquired were marked at a pixel level semantically. The division test consists of 80 videos from eleven patients and 10,709 frames. The training set includes all frames from the remaining videos. The video-based predictor is then trained and evaluated using 5-fold cross-validation (entire movies from the matching patient on that identical fold). The evaluated performance of the proposed frame-based scoring method achieves an average accuracy of 71.4%, whereas video-based score prediction(uni-norms) achieves an 60% F1score, 60% precision, and recall. Pixel-based semantic segmentation for the ensemble of UNet, UNet++, and DeepLabV3 using online augmentation achieves the highest accuracy of 96%, dice-coefficient for unification Covid19 related score of 75%, and mean dice score of 65%.

Born et al. [26] created an ultrasound frame-based approach in Jan. 2021 that correctly separates Covid19 LUS recordings from healthy, pneumonia individuals. The system used five CNN variants(VGG16, VGGCAM, UNet, UNet++, DeepLabV3+). The collected dataset [53]

contains more than 200 LUS convex, linear videos, including 70 videos and 22 images for Covid19 class, 51 videos and 22 images for bacterial pneumonia class, 6 videos for viral pneumonia class, 73 videos, and 15 images for healthy class. Also, the author has released the same dataset on the public platform. The system used only three classes; it excluded the viral pneumonia class for the analysis due to the small amount of instances (3 convex-videos). Later, manually handled all convex LUS data, including 179(videos), 53(images), and divided the videos into frames at a frame rate of 3 Hz (maximal 30 frames/video). The final analysis dataset leads to a database of 1204 frames of Covid19, 704 frames of bacterial pneumonia, and 1326 healthy classes. All frames were rescaled to 224 × 224 pixels. Outcomes were attained in 5-fold cross-validation by sample numbers per class. The suggested frame-based model with VGG provides the best performance for the Covid19 class, with metrics of 88% recall, 90% accuracy, 89% F1 score, and 94% specificity. Whereas VGG-CAM obtains 90% recall, 92% precision, 91% F1-score, and 96% specificity for video-based outperformance, the Genesis model achieves 74% recall, 77% precision, 75% F1-score, and 87% specificity.

Furthermore, Muhammad and Hossain [108], in Aug. 2020, proposed a classification of Covid19 in healthy individuals using multi-layers fusion from LUS. The proposed model is a light CNN network containing fewer than 0.4 million learnable parameters. Then extracted features from diverse layers were merged to create a feature vector to be served into MLP, using FC-layer, for classification. The dataset collected from [28] contains 121 videos, including 45(Covid19), 23(bacterial-pneumonia), 53(normal), other 40 frames containing 18(Covid19), 7(bacterial pneumonia), and 15(normal) classes. Frames with a resolution of 512 × 512 pixels were used in the experiment. The proposed fusion method with ResNet, SqueezeNet, achieves 92.5% precision and 91.8% accuracy. Rojas-Azabache et al. [136] proposed DL-based recognition of Covid19 illness from LUS images. The dataset was obtained from a different private health clinic in Lima and consisted of 50 LUS videos, from which 750 frames were mined for situations with Covid19 and 750 frames for the healthy class. Grayscale frames with 512 × 512 pixels were available. The dataset was categorized into Covid19 and healthy classes. The experimental results were 100% accurate. A profound learning classifier for recognizing Covid19 using LUS frames was produced in another investigation by ArntField et al. [11]. Model has been trained on LUS-frames through B-lines using various etiologies. The dataset was collected from LHS-center 2 hospitals and consists of 600 LUS videos (121,381 frames) classified as Covid19, nonCovid severe lung suffering illness (nonCovid), and hydrostatic pulmonic edema (HPE). For training, 99,471 frames (500 videos) were considered, and for test-1, 9540 frames (49 Videos), and for test-2, 12,370 frames (63 videos) were evaluated. The proposed system achieves 100% AUC for Covid19, HPE class, whereas 93.40% for nonCovid class.

5.2 Real-world hybrid & custom deep learning methodologies, evaluations with recent schemes

Born et al. [27], in Jan. 2021, proposed spontaneous recognition of Covid19 from ultrasound images. The proposed LUS model (POCOVID-Net) used VGG16 as its backbone. The large dataset was collected and made publicly available on [28] called POCUS. The method analyzed 1103 images from 64 videos, including 654 frames of Covid19, 277 frames of bacterial pneumonia, and 172 frames of healthy controls. The system implemented using 5-fold cross-validation. The POCUS contains a total of 2,392,963 trainable and 12,355,008 non-trainable parameters. The POCOVID-Net model achieves an average accuracy of 89%.

Whereas for the Covid19 class, the POCOVIDNet model with five-fold cross-validation achieves 96% sensitivity, 79% specificity, 88% precision, and 92% F1score. The recent study [17] in Nov. 2022, implements LUS-based COVID19 classification utilizing the combination of custom graph+Capsule NN. The experimental simulation trained on single POCUS [28] datasource containing 1560 samples of COVID19, pneumonia, and healthy labels. In comparison between capsule and graph network, the graph module performed well w.r.t. classification accuracy. The capsule attained 95.21% accuracy whereas the graphs network attained 97.26% accuracy, 96.93% AUC, 95.92% F1-score, and (93.11, 98.68) CI.

In addition to the above theoretical classification explanation, we have *tabularized the continuing(apart from the above-discussed systems) Covid19 detection methods in* Table 2. Table 2 shows the critical traits of technical and numerical analysis, such as datasets, network, samples/label, data splitting criteria, and the quantitative performance of the examined Covid19 diagnosis systems. It also classifies the different imaging modalities using pretrained, hybrid/custom-made models with DML.

6 COVID-19 classification using paper-based ECG-trace images and genome sequencing

6.1 Genome sequence for COVID-19 classification

To classify the coronavirus genomic information, a novel concept called Neurochaos Learning (NL) was introduced by Harikrishnan et al. in 2022 [61]. The scientific findings of chaotic and inhomogeneity at the scale of neurons in biological brain circuits served as the inspiration for NL. The authors assembled multisource dataset [1, 123] for collecting RNA strands. A multilayer structure made up of chaotic neurons makes up the NL-framework. When employing leaving one out cross-validation, the mean 0.998 sensitivity, 0.998 specificity, 0.998 accuracy for NL for the multiclass classification issue (SARSCoV2, Coronaviridae, Metapneumovirus, Rhinovirus, and Influenza). The evaluation performance demonstrates a mean macro F1-score greater than 99 for the recognition of SARSCoV2 and 1 genome analysis using just single trained model per subclass for 1000 separate randomized train sessions. The effectiveness of NL is compared to that of KNN, LR, RF, SVM, and NBC classifiers. A concentricity method to categorise the SARSCoV2 utilising comparable DNA created with the single-stranded RNA virus, is presented in another paper by Singh et al. [151]. 1582 cases in aggregate, with varying genomic scenes sizes across distinct areas, was gathered from multiple data sources and split into SARSCoV2 and nonSARSCoV2 groups. Applying DSP approaches, we isolated eight biomarkers depending on three frequency, and we ordered them employing a filter-based attribute extraction. The ranking markers were employed as input for the KNN, SVM, DT, and RF algorithms to distinguish SARSCoV2 against different coronaviruses. Through 10-fold-validation, the effectiveness of the predictors depending on correctness and F-measure was evaluated using the trained model. After being evaluated using unknown data, RF was determined to be the most accurate classifier, discriminating the SARSCoV2 virus from other coronaviruses and control subjects with 97.4% accuracy, 96.2% sensitivity, and 98.2% specificity. Additionally, the suggested approach outperformed earlier research in terms of combinatorial efficiency, computing the genomic indicators in just 0.31 s.

Table 2 Remaining models (apart from the above theoretical descriptions) summary of Covid-19 X-ray, CT, and ultrasound classifications

Ref.	Type	Network Names	Size	Total Instances	Sample Size/Class
Verma et al. [160]	Pre-trained (X-ray)	VGG-16, ResNet-50, InceptionV3, EfficientNet CNN	224×224	852	426 (Covid19 positive), 426 (Covid19 negative)
Khan et al. [90]	Pre-trained (X-ray)	CoroNet (Xception)	224×224	1251	310(Healthy), 330 (Pneumonia bacterial),327 (Pneumonia viral), 284 (Covid19)
Karhan et al. [86]	Pre-trained (X-ray)	ResNet50		1200	200(Covid19), 1000 (Non-Covid19)
Zebin et al. [170]	Pre-trained (X-ray)	VGG16, ResNet50, and EfficientNetB0	224×224	802	202 (Covid19), 300 (Normal), 300 (Pneumonia)
Saiz et al. [143]	Pre-trained (X-ray)	VGG-16, SDD300		1500	204 (Covid19), 649 (Normal), 647 (Pneumonia)
Mostafiz et al. [107]	Custom (X-ray)	DWT & CNN	224×224	4809	790(Covid19),1215 (Viral-pneumonia), 1304 (Bacterial-pneumonia), 1500 (Normal)
Salman et al. [144]	Pre-trained (X-ray)	VGG16, ResNet50, InceptionV3		260	130 (Covid19), 130 (Normal)
Majeed et al. [101]	Hybrid (X-ray)	CNN-X(VGG16/19, GoogleNet,ResNet18/ 50/101, InceptionV3, Inception ResNetv2, SqueezeNet,DenseNet 201, Xception, AlexNet	224×224	6024	1575 (Normal), 2771 (Bacterial pneumonia), 1494 (Viral pneumonia), 184 (Covid19)
Sevi et al. [148]	Pre-trained (X-ray)	CNN, VGG, VGG19, InceptionV3	299×299	657	219 (Covid19), 219 (Healthy), 219 (Viral pneumonia)
Togaçar et al. [158]	Pre-trained (X-ray)	MobileNetV2, SqueezeNet	224×224	458	295 (Covid19), 65 (Normal), 98 (Pneumonia)
[19]	Ensemble (X-ray)	PULDI-COVID	Variable Size	10,800	1200 labels/class(Atelectasis,Bacterial,Covid19, Cardiomegaly,Effusion,Infiltration,NoFinding, Pneumothorax,Viral)
[21]	Custom (X-ray)	LDC-NET	1024×1024	10,800	1200/class(Atelectasis,Bacterialpneu, Cardiomegaly, Covid19,Emphysema,Fibrosis,Healthy, Tuberc-ulosis,iralPneu.)
Zhang et al. [171]	Pre-trained (CT)	VB-net		2460	2460 (Covid19)

Table 2 (continued)

Ref.	Type	Network Names	Size	Total Instances	Sample Size/Class
Kalane et al. [85]	Pre-trained (CT)	U-Net	512×512	1000	448 (Covid19), 552 (Normal)
Jaiswal et al. [77]	Pre-trained (CT)	DenseNet201		2492	1262 (Covid19 +), 1230 (Covid19 -)
He et al. [62]	Custom (CT)	MNas3Dnet41	160×160	340,190	152,791(Corona virus pneumonia), 157,940 (Common pneumonia), 87,214 (Normal)
Alakus et al. [7]	Pre-trained (CT)	ANN, CNN, LSTM, RNN, CNNLSTM, CNNRNN		600	80 (Covid19), 520 (No-findings)
Gozes et al. [57]	Pre-trained (CT)	U-Net, ResNet50	224×224	1865	1036 (Normal), 829 (Covid19)
[17]	Custom (CT)	Capsule Convolution Neural Net	512×512	10,000	2500/(Covid19, LungCancer, Pneumonia,Healthy)
[17]	Custom (LUS)	Graph Neural Net	512×512	1560	Covid19,Pneumonia,Healthy
Roy et al. [139]	Pre-trained (LUS)	CNN, Regularized Spatial Transformer Networks (Reg-STN), SORD,Unet, Unet++, Deeplabv3+	260×200	58,924 Frames	5684 (Score 3), 18,972 (Score 2), 14,295 (Score 1), 19,973 (Score 0)
Born et al. [26]	Pre-trained (LUS)	VGG-16, VGG-CAM, U-Net, U-Net++, DeepLabv3+	224×224	202 Video s+59 Images	1204 (Covid19), 704 (Bacterial Pneu.), 1326 (Healthy)
Muhammad & Hossain [108]	Pre-trained (LUS)	ResNet50, SqueezeNet	512×512	121 Videos, 40 Images	Image:18(Covid19), 15(Healthy), (Bacte rial-pneumonia) Video: 45(Covid), 53 (Healthy), 23(Bacterial-pneumonia)
Rojas-Azabache et al. [136]	Pre-trained (LUS)	VGG-16	224×224	50 Videos	750 (Covid19), 750 (Healthy)
Arntfield et al. [11]	Pre-trained (LUS)	Xception	600×600	600 Videos	DND
Born et al. [27]	Hybrid (LUS)	POCOVID-Net(VGG-16)	224×224	1103 Images (64 Videos)	654 (Covid19), 277 (Bacterial pneumonia), 172 (Healthy)

Table 2 (continued)

Ref.	Data Partition	Performance Evaluation	Datasource Reference	Test Time/image
Verma et al. [160]	Random	Accuracy:90.45%, Specificity:73.20%, Sensitivity:81.20%	COVIDGR 1.0 dataset	DND
Khan et al. [90]	4-fold cross-validation	Accuracy:99%, Precision:98.3%, Recall:99.3%, Specificity:98.6%, F-measure:98.5%	[54, 83]	DND
Karhan et al. [86]	5-fold cross-validation	Accuracy:99.5%	[36, 37, 54, 83]	DND
Zebin et al. [170]	Training:70%, Testing:30%, Validation: 5-fold cross-validation (augmented)	Accuracy:96.8%, Precision:100%, Recall:97.50%	[54, 83]	18 s
Saiz et al. [143]	Testing:34.2% (513 images), Training:65.8% (987 images)	Accuracy:92.00%, Sensibility:94.92%, Specificity:92.00%	[54, 129]	13 s per image
Mostafiz et al. [107]	Training:70%, Testing:30%, 5-fold cross-validation	Accuracy:99.45%, Precision:97.51%, Recall:99.17%, F1-score:98.33%	[39, 54, 89]	DND
Salman et al. [144]	Training:60%, Testing:20%, Validation:20%	Accurary:100%	[30, 54, 83]	DND
Majeed et al. [101]	Random	Sensitivity:93.15%, Specificity:97.86%	[39, 54, 89]	DND
Sevi et al. [148]	DND	Accuracy:95%, Precision:100%, Recall:93%, F1-score:96%	[38]	DND
Togaçar et al. [158]	Training:70%, Testing:30%, 5-fold cross-validation	Accuracy:99.34%, Sensitivity:99.32%, Specificity:99.37%, Precision:99.66%, F-score:99.49%	[5, 38, 54]	DND
[19]	Train:80%, Valid:10%, Test:10%.	Accuracy:99.70%, Precision:98.68%, Recall:98.67, F1score:98.67, AUC:99.24%	[83, 116, 149]	8.59 s
[21]	Train:80%, Valid:10%, Test:10%.	Accuracy:99.28%, Precision:96.86%, Recall:96.78%, F1-score:96.77%,	[38, 42, 54, 83, 116]	0.136 s
Zhang et al. [171]	DND	Accuracy:90%	Huoshenshan Wuhan Hospi, [56]	DND
Kalane et al. [85]	10-fold cross-validation	Accuracy:94.10%, Sensitivity:94.86%, Specificity:93.47%, Precision:95%	[37, 40, 54], ISMIR	1.06 s
Jaiswal et al. [77]	Training:68%, Testing:15%, Validation:17%	Accuracy: 97.4%	[56]	DND
He et al. [62]	Training:80%, validation:20%	Accuracy:87.14%, F1-score:87.25%, AUC:95.70%	Clean-CC-CCII [52]	DND
Alakus et al. [7]				DND

Table 2 (continued)

Ref.	Data Partition	Performance Evaluation	Datasource Reference	Test Time/image
	Training:80%, Testing:20%, 10-fold cross-validation	Accuracy:92.30%, F1-score:93%, Precision:92.35%, Recall:93.68, AUC:90%.	Hospital Israelita Albert Einstein at Sao Paulo Brazil	
Gozes et al. [57]	Random	AUC:99.40%, Sensitivity:94%, Specificity:98%	El-Camino Hospital(CA), Zhejiang province, China, Univ. Hospitals Geneva	DND
[17]	Train:80%, Test:10%. Valid:10%	AUC:98.93, Accuracy:99.2, F1-Score:98.4, Sensitivity:98.4 Specificity:98.4	[52, 157]	DND
[17]	Train:80%, Test:10%. Valid:10%	AUC:96.93 Accuracy:97.26, F1-Score:95.92 Sensitivity:95.90	[28]	DND
Roy et al. [139]	Frame: Train:80%, Test:20%. Video:5-fold cross-validation	Accuracy:96%, F1-score:61%, Precision: 60%, Recall:60%	[74]	DND
Born et al. [26]	5-fold cross validation	Recall:90%, Precision:92%, F1-score:91%, Specificity:96%	DND	DND
Muhammad & Hossain [108]	5-fold cross validation	Accuracy:91.8%, Precision:92.5%	[28]	DND
Rojas-Azabache et al. [136]	DND	Accuracy:100%	Private clinics of Lima	DND
Arntfield et al. [11]	Train:80%, Test:20%.	AUC:100%	LHSC 2 tertiary hospitals	DND
Born et al. [27]	5-fold cross-validation	Accuracy:89%, Sensitivity:96%, Specificity:79%, Precision:88%, F1-score:92%	[28]	DND

Note: DND: indicates the specific author has not disclosed the parameter's value, LUS: Lung Ultrasound.

6.2 Paper-based ECG-trace images for COVID-19 classification

In response to the issues the COVID19 infection causes in pulmonary circulation, a unique DCNN method is presented by Irmak [71] in 2021. For the assessment of COVID19 illness by employing just ECG tracing pictures produced with ECG impulses of COVID19 affected individuals. The single source ECG-trace dataset [91] contains 650 COVID19, 300 MI(Myocardial Infarction), 720 healthy, 600 irregular heart pulses samples. ECG-trace dataset details are tabulated in Table 1. The whole 2170 ECG dataset is divided using classical hold-out method in ratios of 60–20-20%. For the 2-class objectives of (COVID19/Healthy), (COVID19/Irregular heart-rate), and (COVID19/MI), the aggregate classification accuracy of 98.57%, 93.20%, and 96.74% and AUC score of 99.6, 97.7, and 99.05 are obtained, consecutively. Additionally, for the 3-class(COVID19, Irregular Heart rates, MI) and 4-class(Healthy, COVID19, Irregular Heartbeats, MI) classification problems, average classification accuracy of 86.55% and 83.05%, respectively, were attained. Furthermore, in addition to above study, ECG-based COVID19 detection using multi-DCNN ensemble approach was suggested by [20] in Nov. 2022. The simulation utilizes 4 base models(VGG16,DenseNet201, MobileNetV2,ResNet152V2) and 11 meta/ensemble models. The pair of [M2, M3] and [M1, M2, M3] offers well similar results with 93.5% accuracy, 87% recall, 87.03% F1score, and 95.67% specificity 95.67.

7 Segmentation approaches used for COVID-19

We also reviewed some segmentation-based articles to comprehend the segmentation of Covid19 lung-infected regions. After adjusting the general intensity, the edge of the diseased lung may be improved. Image segmentation can be accomplished in two methods. The first step is to mine features above an image patch. The second step is to train using a labeled data set approach. The DL can employ either traditional CNN over image patches or FC networks across the entire image. Jiang et al. [81], in Feb. 2021, suggested a dual-generator structure (global-local) and dual-discriminator (multi-resolution) for Covid19 CT image fusion using conditional-GAN. A dual generator is used to report and replicate different stages of information from CT. A dual discriminator aimed at learning at full-FR (512 × 512) and half-HR (256 × 256) resolution CT data. GAN was used to learn to differentiate input as original or forged. A DESUM at the generators helps to equilibrium the lung part and minor injury region data by energetically weighing two positions through the element-wise totality method and stopping the generator from being excessive. A DFM was at the discriminator for weighing the loss from 2 inputs with different resolutions. It also permits the HR discriminator to obtain additional lung structure or injury region data. It also deals with additional features of minor injury areas to the FR discriminator. These twin multiple discriminators assisted in alleviating training procedures and increased the appearance feature of artificial data. Such techniques could be efficiently used for data augmentation tasks to help trainee radiologists who want great snapshots of Covid19 samples and semantic segmentation for Covid19 chest radiography digital imaging. The network of the global info-generator utilizes a 4-convo-layer with ReLU for upsampling and downsampling and 9-res-blocks. The system used 829 lung CT samples from radiopedia [36] database. Experimented synthesis segmentation for Covid19 infection achieved a 90.19% dice score, 90.34% sensitivity, and 99.84% specificity.

For automatic segmentation of Covid19 infected areas and entire lung CT Chest scan Yan et al. [168] in Mar. 2021 proposed a 3D-convolution-based DL structure called Covid-SegNet. The used dataset contains 165,667 annotated 861 scans of Covid19 patients. A total of 731 individuals CT were arbitrarily selected for training. For the testing set, 130 patients. The proposed feature variation(FV) block efficiently improves the ability of feature demonstration for the Covid19 infected segment. By injecting the features at changed measures by offering progressive atrous spatial pyramid pooling (PA-SPP) for managing refined contamination regions of various looks and contours. The Covid-SegNet model contains res-blocks, FV-blocks, PA-SSP-blocks, and down sampling for encoding layers and res-blocks and de-convolution layers kernels with a stride of half(1/2) for decoding layers. To generate segmentation results was the responsibility of the last layer. For lung and Covid19 segmentation, the proposed technique attained dice similarity scores of 98.7% and 72.6%, respectively.

The summary report with technical details for experimentation/simulation setup from reviewed articles with detailed values are provide in Table 3.

Complexity of a network is measured using number of layers. The capability of the model rises as the depth increases. Training DL networks, including those with multiple hidden layers, can be more operationally expensive than a single-layer network. Table 3 statistical analysis shows that 16 systems use standard layers, 20 systems employ customized layers, and the remaining 30 systems do not disclose the number of layers they use (Fig. 8a). Almost 92% of the studied systems provided accuracy as the performance metric. A too-high learning rate may force the network to diverge too rapidly to an unsatisfactory result, while a too-low learning rate can lead the system to freeze. The difficulty in training DNN is that the learning rate must be chosen appropriately. Twenty one methods applied the 0.0001 learning rate, which is the highest (shown in Fig. 8c). Kernel size plays a vital role in automatically extracting valuable features from the network for image classification or object detection. From the 62 studied systems, 28 systems use 3 × 3 kernel size (shown in Fig. 8b), batch size from 1 to 512 samples per iteration, and epochs ranging from 5 to 1500 for all systems.

The activation function is added to the network to learn the complex pattern from the data. Thirty-six systems utilize ReLU, 18 systems use softmax, two systems for each sigmoid and Leaky ReLU, whereas Bernoulli, PQIS, and Tanh used once in 3 systems (shown in Fig. 8d). Generally, we employ ReLU in the hiding layers to prevent the critical gradient issue and improve computing speed and Softmax in the final layer. Optimizers are strategies for minimizing an error (loss function). Optimizers are scientific tasks that are based on the learnable parameters of a model, such as weights and biases. Thirty six systems used the Adam optimizer in the studied network (Fig. 8e).

8 Open discussion, challenges, and future trends

8.1 Open discussion

This research aims to identify the best DML architectures for detecting, segmenting, and classifying Covid19. Table 3 summarizes detailed technical analysis outcomes of the individual systems for simulation operations stated in the peer-reviewed papers. Throughout this study, 62 diagnosis methods were surveyed; including X-ray(32), CT(19), 7 systems based on ultrasound, and 4 other CAD systems(ECG, genome sequence). 33 systems used multi-source data, only 16 systems employed a solitary dataset, and the rest system did not disclose the

Table 3 Summary report of experimental setup work with technical details and performance metrics in the studied papers

Author	Model	Layer	Kernel Size	Pool size	Stride, Batch Size	Image Size
Islam et al. [72]	CNN, LSTM	Conv2D: 12, Pool: 5	3×3	2×2	Conv2D:1, Pool:2	224×224
Bassi et al. [13]	DenseNet201	Standard Layer			Batch size:16	224×224
Wang et al. [165]	GoogleNet, Inception v3	Conv:6, Pool:2	3×3	1×1	Conv:2, Pool:1	299×299
Ni et al. [115]	MVP-Net and 3D-Unet					
Jain et al. [75]	ResNet50, ResNet-101,	Standard layer	5×5	1×1	Stride:2, Batch size:32	640×640
Ozcan [121]	GoogleNet, ResNet18, ResNet50	Standard layer	3×3	2×2		224×224
Xu et al. [167]	3D-CNN	Conv:70				256×256
Joshi et al. [82]	CNN, DarkNet-53, YOLO-v3 Arch.	Conv:16, Residual: 5	3×3	1×1	Batch size:16	416×416
Loey et al. [98]	AlexNet, VGGNet16, VGGNet19, GoogleNet, ResNet50, CGAN	Standard layer	5×5		Batch size:32	256×256
Fontanellaz et al. [49]	CNN	Conv:8, Dense:2	3×3	2×2		480×480
Rahimzadeh et al. [132]	ResNet50V2 with FPN, Xception, Resnet50V2				Batch size:14	512×512
Abdani et al. [2]	SPP-COVID-Net(DarkCOVIDNet)	Conv:14, Mp:4,Dense:1, SPP:1	3×3	2×2	Stride:1	1024×1024
Rahimzadeh et al. [131]	Xception and ResNet50V2	Xcept:5, Res:5, Concat:1	3×3	1×1	Batch size:30	
Saeedi et al. [142]	ResNet, Inception, and MobileNet	Standard layer				224×224
Irmak [70]	CNN	Conv:12	7×7	5×5	Stride:4	227×227
Nour et al. [118]	Baysian Algo with CNN	Conv:5, Norm:5, Pool:5, FC:3	9×9		Batch size:128	224×224
Wang et al. [164]	DeCoVNet, Unet	Stem, ResBlock,	7×7	3×3	Batch size:1	368×368
Han et al. [59]	AD3D-MIL, Bernoulli distribution					256× 256
Cruz [63]	VGG16, ResNet50, ResNet50, DenseNet161, DenseNet169, InceptionV3	Standard layer			Batch size:32	256×256
Rafi [130]	ResNet-152, DenseNet-121	Standard layer	3×3		Batch size:24	
Paluru et al. [124]	Anam-net	AD-block:6, Mp:4, Conv:8, Transconv:4	3×3	1×1	Batch size:5	512×512
Panwar et al. [126]	nCovNet(VGG16)	Conv+ReLU+SM:18	3×3	2×2	Conv:1, Pool:2	224×224
Ardakani et al. [10]	ResNet18, ResNet50, Xception ResNet101, VGG16, VGG19, AlexNet, SqueezeNet, GoogleNet, MobileNetV2	Conv:3, Inception:9, Others 22				512×512

Table 3 (continued)

Author	Model	Layer	Kernel Size	Pool size	Stride, Batch Size	Image Size
Nayak et al. [112]	VGG-16, Squeezenet, Inception-V3, AlexNet, MobileNet-V2, ResNet-34	Standard layer	3×3		Batch size:32	Ince-V3: 299×299 others 224×224
Konar et al. [93]	PQIS-Net		1×1	2×2	Batch size:8	512×512
Das et al. [110]	Xception	Conv:18, Pool:4,				299×299
Zhang et al. [171]	VB-net					
Ozturk et al. [122]	DarkNet (DarkCovidNet)	Conv:17, Pool:5			Batch size:8,16, 32	256×256
Narin et al. [111]	ResNet50, ResNet101, ResNet152, InceptionV3, InceptionResNetV2	Standard layer	3×3		Batch size:3	224×224
Kalane et al. [85]	U-Net	Conv:20, Pool:4	3×3	2×2	Conv:2, pool:1, Batch:100	512×512
Pandit et al. [125]	VGG-16	Conv:13, Pool:5,fc:3	3×3	2×2	Batch size:64	224×244
Medhi et al. [103]	CNN	Conv:4, Pool:4	3×3	2×2	Stride:0	
He et al. [62]	MNas3DNet41		3×3		Batch size:64	160×160
Abbas et al. [46]	DeTraC (AlexNet, VGG19, ResNet, GoogleNet, SqueezeNet		3×3			4020×4892, 4248×3480
Jaiswal et al. [77]	DenseNet201	Conv:4, Dense:5, Pool:5	3×3	2×2	Stride:2	
Aslan et al. [12]	mAlexNet,mAlexNet + BiLSTM	Conv:5, FC:9, Pool:3, BiLSTM:2	3×3	3×3	Stride:4, Batch size:60, 512	1024×1024, 227×227
Alakus et al. [7]	ANN, CNN, LSTM, RNN, CNNLSTM, CNNRNN	Conv:3			Batch size:512, 256, 32,16,8	
Verma et al. [160]	VGG-16, ResNet-50, Inception V3, EfficientNet, TL CNN	Standard layer			Batch size:50	224×224
Gozes et al. [57]	U-Net, ResNet50, VGG16	Standard layer	3×3	2×2		224×224
Khan et al. [90]	CoroNet(Xception)		5×5		Batch Size:10	224×224
Karhan et al. [86]	ResNet-50	Standard layer			Batch size:32	
Zebin et al. [170]	VGG16, ResNet50, EfficientNetB0	Standard layer			Batch size:8	224×224
Saiz et al. [143]	VGG-16, SDD300					
Mostafiz et al. [107]	DWT & CNN	Conv:49, pool:1	3×3	1×1		224×224
Salman et al. [144]	VGG16, ResNet50, InceptionV3	Standard layer				
Majeed et al. [101]			3×3	2×2	Stride:3, Batch Size:15	224×224

Table 3 (continued)

Author	Model	Layer	Kernel Size	Pool size	Stride, Batch Size	Image Size
	CNN-X, AlexNet, GoogleNet, Vgg16, Vgg19, ResNet18, ResNet50, ResNet101, InceptionV3, SqueezeNet, InceptionResNetv2, Xception, Densenet201					
Sevi et al. [148]	CNN, VGG16, VGG19, InceptionV3	Standard layer	3×3	2×2		299×299
Togaçar et al. [158]	MobileNetV2, SqueezeNet	Conv: 15	3×3	1×1	Stride:3, Batch size:64	224×224
Roy et al. [139]	CNN, Regularized Spatial Transformer Networks(Reg-STN), U-Net		5×5	2×2	Batch size:64	260×200
Born et al. [26]	VGG-16, VGG-CAM, U-Net, UNet++, DeepLabv3+				Batch size:8	224×224
Muhammad & Hossain [108]	ResNet50, SqueezeNet	Block:5	5×5	2×2	Stride:2, Batch size:5	512×512
Azabache et al. [136]	VGG-16	Conv:13, MP:5, ft.:1, FC:2				224×224
Arntfield et al. [11]	Xception	Standard layer				600×600
Born et al. [27]	POCOVID-Net					224×224
[19]	Puldi-COVID (VGG16/19, ResNet50, DenseNet201–169, MobileNetV2, NASNetMobile, ResNet152V2)	Custom Layer	3×3	2×2	Batch Size: 64	Varying Size
[21]	LightWeight Lung Diseases with COVID19. LDC-Net (Custom DCNN)	Conv:8, MP:8, Ft:1, FC:3	3×3	2×2	Batch Size: 32	1024×1024
[20]	ECG-CCNet (Ensemble VGG16,DenseNet201,MobileNetV2,-ResNet152V2).	Conv:3,4, MP:3,4, FC:2,	3×3	2×2	Batch Size: 32	849×748
[17]	Capsule + Graph convolutional network.	Custom Layer	5×5	2×2	Batch Size: 32, Stride:2	512×512
Harikrishnan et al. [61]	Neurochaos (KNN, LR, RF, SVM, NBC)	ChaosFEX+SVM	RBF kernel			
Singh et al. [151]	DSP(KNN, SVM, DT, and RF), DFT-features	magnitude spectrum, peak-to-average ratio,SVD+ filtering, AMDF+AMDF,-TDP+filtering				
Irmak [71]	ECG, VGG16	Conv:4, MP:4		2×2	Batch Size:32	224×224
Byh [20]	ECG-CCNET (VGG16, DenseNet201, MobileNetV2, ResNet152V2)	Custom Layers	3×3	2×2	Batch Size:32	224×224

Table 3 (continued)

Author	Learning Rate	Epoch	Performance Metrics	Activation function	Optimizer	Software Package / Tools
Islam et al. [72]	0.0001	125	Accuracy:99.2%, Specificity:99.2%, Sensitivity:99.3%, F1-score:98.9%	ReLU		Keras, TensorFlow2
Bassi et al. [13]	0.0001	154	Accuracy of DNNC:100%, DNNA:99.3%, DNNB:98.7%	Softmax		Keras, pytorch, TensorFlow,
Wang et al. [165]	0.01	1500	Accuracy:89.5%, Specificity:88%, Sensitivity:87%	Softmax	SGD	
Ni et al. [115]			Accuracy:93%, AUC:86%, Sensitivity:96%, Specificity:97%			
Jain et al. [75]	0.0001	25	Accuracy:97.77%, Recall:97.14%, Precision:97.14%, Specificity:98.66, F1-score:98.15%	Softmax	SGD	Keras, Tensorflow, pytorch
Ozcan [121]	0.001	81	Accuracy: 97.69%, Precision:95.95%, F1-score:96.60%, Sensitivity:97.26%, Specificity:97.90%			
Xu et al. [167]		1000	Accuracy:86.7%, Precision:81.3%, F1-score:83.9%	Softmax		
Joshi et al. [82]	0.001	250	Accuracy:97.11	Leaky ReLU	SGD	Tensorflow, Keras, OpenCV
Loey et al. [98]	0.001	50	Accurarcy:82.64%, Sensitivity: 88.30%, Specificity:93.33%	ReLU	Adam	MATLAB DL package TensorFlow
Fontanellaz et al. [49]			Accuracy:94.3%, Sensitivity: 97.0%, F1-score:94.3%	ReLU		
Rahimzadeh et al. [132]	0.0001	50	Accuracy: 98.49%	ReLU	Nadam	Colab, Keras, Tensorflow
Abdani et al. [2]	0.0001	100	Accuracy: 94.6%	ReLU	Adam	Keras, Tensorflow
Rahimzadeh et al. [131]	0.0001	800 (100/8)	Accuracy:99.56%,	Softmax	Nadam	Google Colab, Keras
Saeedi et al. [142]			Accuracy:90.61%, Recall:90.80%, Precision:89.76%, AUC:95.05%		Nu-SVM, Bayesian	Tensorflow, Keras, SKlearn.
Irmak [70]		90	Accuracy:99.20%, Specificity 98.41%, Sensitivity 100%, Precision 98.41%,	Softmax, ReLU	SGDM	Matlab R2019a
Nour et al. [118]	0.0001	64	Accuracy:98.97%, Sensitivity:89.39%, Specificity:99.75%, F1-Score:96.72%.	ReLU	Bayesian optimizer, Adam	MATLAB (2019a)
Wang et al. [164]	0.00001	100	Accuracy:90.10%	ReLU	Adam	PyTorch

Table 3 (continued)

Author	Learning Rate	Epoch	Performance Metrics	Activation function	Optimizer	Software Package / Tools
Han et al. [59]	0.00001	100	Accuracy:97.9%, AUC:99.0%, Cohen kappa score:95.7%.	Bernoulli distri.	Adam	Pytorch
Cruz [63]	0.001	30	Accuracy:86.70%, F1- score:85.86%, AUC:90.82%	ReLU	AdamW, SGD	Keras
Rafi [130]	0.00001	30	Accuracy:98.43%, Specificity:99.23%, Sensitivity:98.71%.	ReLU	Adam	PyTorch
Paluru et al. [124]	0.00001	100	Accuracy:98.80%, Specificiy:99.70%, Sensitivity:91.10%.	ReLu	Adam	PyTorch, TensorFlow Lite
Panwar et al. [126]	0.0001	80	Accuracy:97.97%, Sensitivity:97.62%, Specificity:78.57%.	ReLU	Adam	
Ardakani et al. [10]	0.01		Accuracy:99.51%, Sensitivity:100%, AUC:99.4%, Specificity:99.02%, PPV:99.27%, NPV:100%		SGDM	
Nayak et al. [112]	Optimal Learning Rate	50	Precision:96.77%, Specificity: 96.67%, F1-score:98.36%, Accuracy:98.33%, AUC:98.36%.	ReLU	SGD, Adadelta, RMSProp, Adam	
Konar et al. [93]	0.01	50	Accuracy:98.4%, Precision:98.6%, Recall:98.5%, AUC:97.8%, F1-Score:98.3%.	PQIS-Net Fun.	SGDM, Adam	MATLAB 2020a, Pytorch
Das et al. [110]			Accuracy:97.40%, F-measure:96.96%, Sensitivity:97.09%, Specificity:97.29%, Kappa-Statistics:97.19% .	ReLU		
Zhang et al. [171]			Accuracy:90%			
Ozturk et al. [122]	0.0001	100	Accuracy:98.08%, Sensitivity:95.13%, Specificity:95.30%, F1-score:96.51%.	Leaky ReLu	Adam	
Narin et al. [111]	0.00001	30	Accuracy:99.7%	ReLU	Adam	Google Colaboratory
Kalane et al. [85]		100	Accuracy:94.10%, Sensitivity:94.86%, Specificity:93.47%	Softmax, ReLU		MATLAB R2019a
Pandit et al. [125]	0.001	25	Accuracy:96%, Sensitivity:92.64%, Specificity: 97.27%	ReLU	Adam	
Medhi et al. [103]			Accuracy:93%	Softmax, ReLU		
He et al. [62]	0.001	200	Accuracy:87.14%, F1-score:87.25%, AUC:95.70%		Adam	
Abbas et al. [46]	0.001	5		ReLU	SGD	MATLAB 2019a

Table 3 (continued)

Author	Learning Rate	Epoch	Performance Metrics	Activation function	Optimizer	Software Package / Tools
			Accuracy:97.35%, Sensitivity:98.23%, Specificity:96.34%.			
Jaiswal et al. [77]	0.001	300	Accuracy: 97.4%	ReLU		
Aslan et al. [12]	0.001	100, 200	Accuracy:98.70%, Recall:98.76%, Specificity:99.33%, Precision:98.77%, F1-score:98.76%	Softmax, ReLU, Tanh, Sigmoid	SGDM, Adam	Matlab
Alakus et al. [7]	0.001	250	Accuracy:92.30%, F1-Score:93.00%, Precision:92.35%, Recall: 93.68, AUC:90.00%.	ReLU	SGD	
Verma et al. [160]	0.0001, 0.0004	10	Accuracy:90.45%, Specificity:73.20%, Sensitivity:81.20%	ReLU	RMSProp, Adam	Google Colab 32 GB RAM.
Gozes et al. [57]	0.0001		AUC:99.40%, Sensitivity:94%, Specificity:98%	ReLU, Sigmoid	Adam	
Khan et al. [90]	0.0001	80	Accuracy:99%, Precision:98.3%, Recall:99.3%, Specificity:98.6%, F-measure:98.5%	ReLU	Adam	Google Colab
Karhan et al. [86]	0.0003		Accuracy:99.5%	ReLU	Adam	
Zebin et al. [170]	0.0001	50	Accuracy:96.8%, Precision:100%, Recall:97.50%	Softmax	Adam	TensorFlow, Keras, PyTorch, sklearn, OpenCV
Saiz et al. [143]			Accuracy:92.00%, Sensitivity:94.92%, Specificity:92.00%	ReLU		
Mostafiz et al. [107]			Accuracy:99.45%, Precision:97.51%, Recall:99.17%, F1-score:98.33%		mRMR + RFE	
Salman et al. [144]		20				Google Colaboratory
Majeed et al. [101]	0.0003	20	Sensitivity:93.15%, Specificity:97.86%	ReLU	Adam	MATLAB version 2019b
Sevi et al. [148]			Accuracy:95%, Precision:100%, Recall:93%, F1-Score:96%	ReLU, Softmax	Adam	Tensorflow Keras
Togaçar et al. [158]	0.00001	20	Accuracy:99.25%, Sensitivity:100%, Specificity:97.78%, Precision:98.88%, F-score:99.44%	ReLU	SGD	MATLAB 2019b
Roy et al. [139]	0.0001	120	Accuracy:96%, F1-Score:61%, Precision: 60%, Recall:60%	ReLU	Adam	
Born et al. [26]	0.0001	40		ReLU	Adam	TensorFlow

Table 3 (continued)

Author	Learning Rate	Epoch	Performance Metrics	Activation function	Optimizer	Software Package / Tools
			Recall:90%, Precision:92%, F1-score:91%, Specificity:96%			
Muhammad & Hossain [108]	0.0001	150	Accuracy:91.8%, Precision:92.5%	ReLU	Adam	MATLAB (R2020a)
Azabache et al. [136]			Accuracy:100%			
Arntfield et al. [11]	0.001	15	AUC:100%	Softmax	Adam	
Born et al. [27]	0.0001		Accuracy:89%, Sensitivity:96%, Specificity: 79%, Precision:88%, F1-score:92%	ReLU	Adam	
[19]	0.0001, reduced LR	150	Accuracy:99.70%, Precision:98.68%, Recall:98.67, F1score:98.67, AUC-ROC score:99.24%	Softmax	Adam	Tensorflow
[21]	0.0001	35	Accuracy:99.28%, Precision:96.86%, Recall:96.78%, F1-score:96.77%,	Softmax	Adam	Tensorflow
[20]	0.00001	75	Accuracy:93.5%, Recall:87%, F1-score:87.03%, Specificity:95.66%, Precision:87.16%, AUC:95.33%	Softmax	Adam	Tensorflow
[17]	0.0001	70	CT(Accuracy:99.2%, Fscore:98.4%), LUS(Accuracy:97.26%, F1score: 95.92%)	Softmax + Graph Node, Edge	Adam	Tensorflow, Keras
Harikrishnan et al. [61]			Accuracy:99.8,Sensitivity:99.8,Specificity:99.8,			LinearSVC, Numba, Numpy Scikit-learn
Singh et al. [151]			Accuracy:97.4%, Sensitivity:96.2%, specificity:98.2%.			MATLAB (R2015a)
Irmak [71]	0.001, 0.0001		Accuracy: 83.05% (4-class)	Softmax	Adam	Matlab R2019a
Byh [20]	0.00001	Varible Epoch Sizes	Accuracy:93.5%, Recall:87%, Fscore:87.03%, specificity: 95.67%	Softmax	Adam	Google Colaboratory

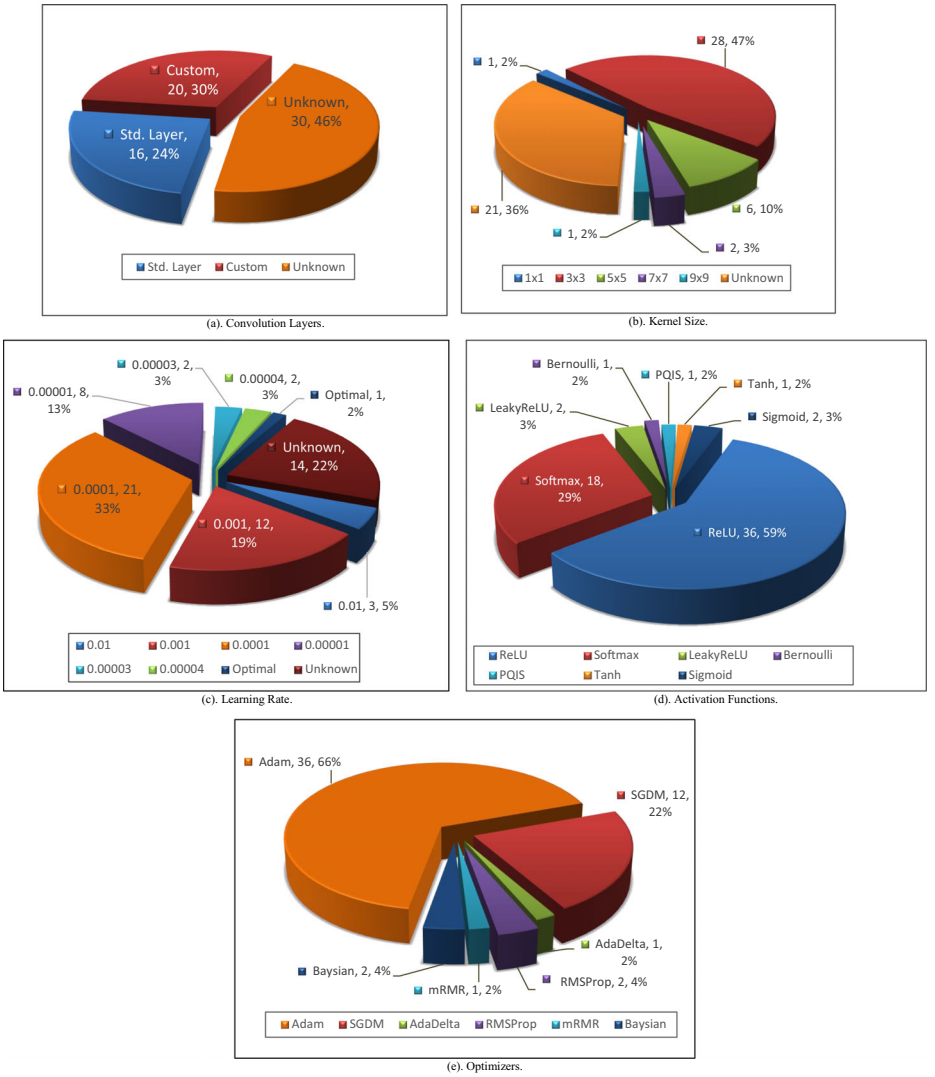

Fig. 8 Statistical analysis of simulation setup with technical details

dataset from the planned system. Covid19 is supported by the usage and necessity of massive records with an accurate highest diagnostic like RT-PCR, and results like mortality and duration for discharge are ubiquitous to DL approaches for imaging Covid19 [43]. The benchmarking datasets or real-world datasets as output from the medical ecosystem are inputs to DL models shown in Table 1. Although a few frameworks included a large dataset [62, 139], the quantity of Covid19 instances is quite small [86, 110, 122, 126]. All across the assessment, the binary [7, 57, 77, 85, 86, 144, 160] and multi-class [90, 101, 107, 170] methods were found. Incorporating medical data, perhaps in time series including repetitive images, vital elements, and blood tests, may be preferred to increase training samples

substantially [150 to 162]. Several investigators and radiological reports have publicly released Covid19 imagery datasets. Theoretically, we summarized the recognized systems by factoring in some characteristics such as datasets, class-wise range of samples, data splitting strategies, the DL approach utilized for detection, and finally, the assessment methods for performance measurement. Also, we tabulated technical and numerical analysis of the remaining systems, which highlights the critical aspects in Table 2. In terms of data splitting, various models used 4-fold to 10-fold cross-validation methods [72, 75, 85, 86, 90, 111], whereas others utilized a specific ratio approach [11, 77, 143, 144] for both the pretrained and custom DML frameworks.

The confusion matrix [159] is a performance-assessment tool for ML-based classification problems with two or more classes as output. Across the study, typical assessment metrics such as accuracy, sensitivity, specificity, precision, recall, F1score, AUC, PPV, NPV, kohen-kappa score, etc., are used. In terms of individual highest performance, 100% accuracy [136], 100% AUC [11], 99.44% F1-score [158], 100% sensitivity [70, 158], 99.75% specificity by [118], and kappa statistics of 98.08% by [110]. By a factor of 30, the X-ray [54] collection is the most utilised resource. The model created in [82] achieved 99.81% accuracy for 2-class and 3-class classification, with the highest accuracy of 99.34% achieved by [158], and for 4-class classification, the highest accuracy was 99% by [90]. The system created in [110] reached 99.52% accuracy for training and 97.50% for the testing phase; the majority of the created techniques resulted in higher precision and the next in terms of sensitivity. The Covid19 cases in the reviewed systems, which used the highest of 152,791 samples and lowest of 80 samples for the experiment, are [62, 160], respectively. Most of the created methods did not disclose the computation time because they employed various data sources for the study; however, some solutions estimated the computing time. The highest time required by the hybrid mAlexNet+BiLSTM [12] model is 224 s, whereas the least execution time(seconds/image) was 1.06 s, 0.136 s seconds by [21, 85]. However, the computation time for a custom model depends on the number of layers and hardware specifications. 90% of researchers did not include the model computation time required for testing/training/ validation based on their hardware configuration. The system developed by [82] using pre-trained networks has taken 0.137 s per image, which is the least execution time for Covid19 detection.

Many of the assessed strategies outperformed the pre-trained network as compared to the custom. The effectiveness of the created DML-network differs (depending on the parameters, layers, sizes, etc.) and therefore is not comparative because various data sizes were utilized practically in each study. When comparing imaging modalities, the X-ray fared better than CT, ultrasound, and ECG. The primary challenges in medical imaging [97, 152] are the quasi-technique of gathering imagery data. Hence, it has been witnessed from the research papers that the diagnosis of Covid19 illness, finding the anomalies for chest radiological images like CT, X-ray, and ultrasound scans show an essential part, and image handling with DL algorithms can make it feasible. The systems in the studied papers are resource-greedy for computation and data sources. However, unique methods for a flow of structural design are required for lung segmentation, feature mining, and the detection of specific injury regions on the lung. Those boundaries motivated us to point toward a novel technique for discovering Covid19 illness with minimal resources in collaboration with real-time radiologists [125].

The CT scan-based Covid19 identification method is time-consuming and laborious, necessitating the professionals participation. CT scanning equipment is challenging for Covid individuals since the patients must frequently be relocated to the CT laboratory. The equipment must be thoroughly cleaned, and there is an increased risk of radiation exposure. While CT

also isn't indicated as a major treatment technique, it's been utilized successfully as a supplementary tool for Covid19 mapping [64]. Like traditional X-ray imaging, CT scans employ X-ray as infrared radiation, but they provide far high temporal contrast due to a much more controlled X-ray beam used to make cross-sectional pictures of the subject. CT is commonly recognized as the primary imaging modality for lung tissue and is universally recognized as the gold standard by doctors. The data engineer [120] has to study and observe doctors' internal findings and medical observations [167]. The radiologist has to gain a structural and functional knowledge of radiological images of Covid19, pneumonia, and normal patients. Because every imaging method varies in conditions of price tag, accessibility, and the scale of medical skill essential to precisely interpret the produced radiography pictures [64], X-ray and ultrasound can be useful at a low price, portability, and used at the bedside. But the CT scan machine is substantially immovable at an extraordinary cost and is accessible inside the boundaries of hospices and medicinal clinics. Globally ~30,000 CT machines exist [27]. Medical image investigation approaches are extremely subtle to dissimilarities of image intensities. According to the study [27], an automatic modeling tool's effectiveness demands that "the luminance of the same tissue must always be equal inside one picture but not differ with tissue position." Almost all photos inside the example data sets must have equal intensity for the same tissues across the board and within a single picture.

According to Hassan et al. [66], the collected necessary information from clinicians to understand the dissimilarity among normal, Covid19, pneumonia-viral, pneumonia-bacterial from X-ray radiography images are:

A) In coronavirus, affected X-ray radiography lung samples found that lung inflation is characterized by greater transparencies of the lung region and fewer broncho-vascular lines than elsewhere in the healthy lung. It's also produced by restricted inhaled air, which tiny airflow limitations can make throughout the context of bronchi and bronchiolitis produced by Covid19 contamination. Overinflated lobes are more extensive than average lungs, and the distance between the ribcage is considerable.
B) Non-Covid identification inside an X-ray imaging revealed normal opacity, regular broncho-vascular patterns, and a cardiac proportion with open cardio-phrenic and costo-phrenic degrees. The tracheal is in the center, and gastric gas may be seen underneath the left ribcage. As a result, this X-ray image illustrates a typical chest radiogram.
C) In pneumonia-viral detection, X-ray images found bigger opaqueness dispersed jointly, giving GGO presence, the feature usually detected in viral pneumonia.
D) In the diagnostic of pneumonia-bacterial detection, the X-ray image has a circular hollow region which was discovered throughout the bottom section of the right upper lobe. This suggests aggregation and enhanced broncho-vascular marks on the same side.

Another study [64] of medical observation contains the flaky investigation or opacities that resemble viral pneumonia characteristics are common themes seen in X-ray pictures of Covid19 individuals. No anomalies are found in X-ray images in the initial phases of Covid19. Nevertheless, because the illness continues, Covid19 eventually emerges as a distinctive unilateral patchy infiltration, including the lung's middle, top, and bottom regions, sometimes with indications of condensation. Keeping in mind the potential ECG [20] aspects including availability, dependability, affordability, real-time observation, and safety, a potential high and efficient way to close the diagnostic barrier for COVID19 illness has been developed.

However, corona variants classification can be effectively implemented using single stranded genome sequencing. The new tools developed by [21] for portable IoT deployable lightweight lung disease classification with COVID19. Similarly, the cloud based remote-diagnosis application implemented in [19] will be helpful for radiographer to detect COVID+COPD illnesses in single shot.

8.2 Challenges and future plan

This section discusses the challenges (gap analysis) for detecting and classifying Covid19 using DL models and offers necessary future plans to address those challenges. A gap analysis from the reviewed articles is depicted in Fig. 9.

8.2.1 Challenges

A lack of gold-standard data is one of the significant challenges [98, 167]: Removing already bio-marked images from publicly downloaded datasets [9] also specific imageries comprise verbatim information, which may hamper network forecast [150]. Ultrasound imageries are inclined to be noisy due to the comparatively short penetration of sound waves into organic tissue equated to X-rays [64]. The complex data disproportions are found in the studied papers [13, 63, 98, 167]. The imbalance of data often increases bias through the training stage of DL techniques. The lack of a Covid19 class dataset leads to class imbalance problems.

Based on the different types of pneumonia and other lung diseases: Several authors have merged different types of pneumonia(almost 15) into a single class for classification with Covid19. This leads to a collision between multiple chronic lung diseases and false predictions [37]. There is a chance of overlapping manifestations(biomarkers) of Covid19 with other pneumonia (IAVP) cases, forming pneumonia and eosinophilia Pneumonia [167].

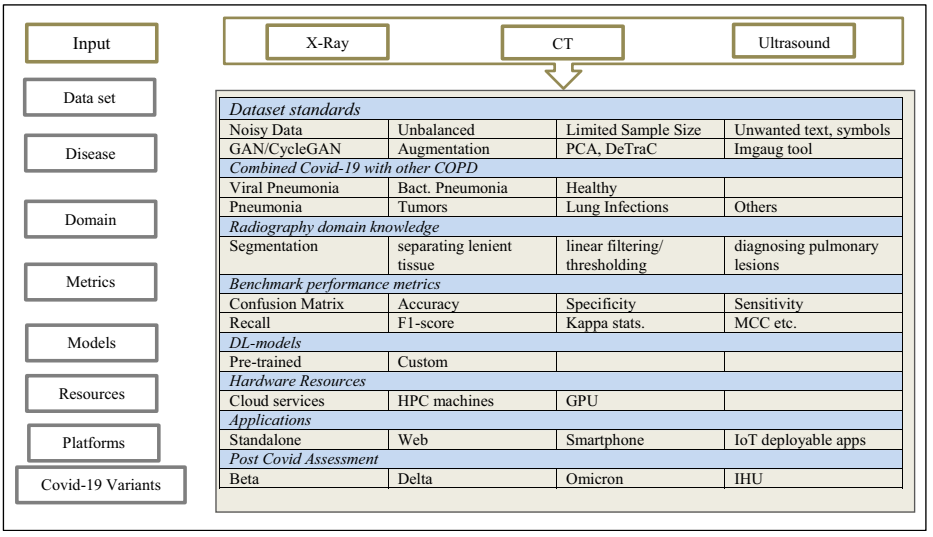

Fig. 9 Obtained gaps as challenges for COVID-19 detection and classification

Medical and radiography domain knowledge Problems in separating lenient tissue produced by low contrast in X-ray imageries have directed confident investigators to improve contrast [3]. It's a pre-processing phase in which radiography-based findings are examined. Furthermore, lung separation of X-ray pictures is critical in diagnosing pulmonary lesions. Several segmentation algorithms rely on linear filtering/thresholding, rolling ball lenses, and, most lately, CNNs [64] have been presented in the research.

Accuracy: To check the robustness of the DL model, it's recommended to train DL architecture having more than ~5500 samples [87]. However, it's observed that from [7, 13, 121, 144, 170], developed systems achieved above 90% accuracy, whereas their Covid19 dataset class was too small(less than 51 samples); this leads to an overfitting DL model. Apart from accuracy, other performance metrics(sensitivity, specificity, F1-score, recall, precision, etc.) need to consider while testing the DL model. Performance evaluation metrics were used in the various studied papers. A confusion matrix is a method of measuring an algorithm's effectiveness. The confusion matrix allows us to see whether the classifier is befuddled when distinguishing between the classes. It is particularly useful for calculating accuracy, recall, precision, specificity, AUC-ROC curves. Mathematical details about benchmark performance metrics are as follows:

$$\begin{bmatrix} TP & \cdots & FP \\ \vdots & \ddots & \vdots \\ FN & \cdots & TN \end{bmatrix} //\text{Confusion matrix}$$

- *True Positive(TP):* The model predicted a positive outcome, and it came true.
- *True Negative(TN):* The model anticipated a negative outcome, and it came true.
- *False Positive(FP), also known as Type 1 Error,* occurs when the model predicts a positive outcome but turns out to be false.
- *False Negative(FN), also known as Type 2 Error:* The model anticipated a negative outcome, but it was incorrect.

a) *Accuracy:* How many of the classes (both positive and negative) have we accurately anticipated?
Accuracy = (TP + TN)/(TP + FP + TN + FN)

b) *Precision:* How many of the accurately anticipated instances were found to be positive?

Precision = TP/(TP + FP)

c) *Recall (Sensitivity):* How many of the actual positive instances might we accurately anticipate using our model?
Recall = TP/(TP + FN)

d) *F-score(F1-score/F-Measure):* Represents the average of precision and recall.

F1-score = 2(Recall*Precision)/(Recall + Precision)*

e) *Specificity:* The proportion of actual negatives, which got predicted as the negative (TP).
Specificity = TN/(TN + FP)

Custom DML models: DarkCovidNet identifies Covid19 quite well for binary categorization. However, there's room to improve in 3-class categorization. This approach requires additional contributions to distinguish Covid19 from several other lung infections [2]. Also, for 3-class classification, the low accuracy shown for Covid19 circumstances is due to the limited number of training images. In [2], the hybrid model manually concatenates the Convo-layers of Xception and ResNet, increasing the model's complexity. The studies expect to design significantly tiny simulations without sacrificing accuracy [2]. Because EfficientNet has a low computing expenditure regarding latencies and memory, it is feasible to use better resolution source imagery to examine increasing the intake resolution on simulation quality [150]. The custom model developed QIS-Net is slower than FC-layers [93]. Subsequently, there is an inequality in dealing with segmentation using QIS-Net and cataloging at the FC layers rather than extracting a (32 × 1).

Hardware resources & computation cost: Another disadvantage of top-functioning approaches seems to be many features that affect both footprints and latencies. Increasing those two measures enables the paradigm to be readily integrated with smartphone apps and IoT devices. Even with a reduced load on servers when provided as a web service, many requests are received from automated Covid19 detection systems every minute. Furthermore, a relatively concise base approach enables more excellent resolution sources while incurring excessively high computing costs. The computation time is an essential component of the general public's exposure too and affordability of technology [150]. There is the possibility of developing lightweight Covid19 detection models which will help deploy on tablets, smartphones, and various handheld devices to achieve portability without worrying about memory and processing/computing power [2]. The studies [12, 46, 85] used a personal laptop or desktop for experimentation. LUS remains comparably understudied compared to other modalities due to a scarcity of structure. DL networks have struggled with well-labeled LUS sets and a total absence of significant data in its minimalist, artifact-based images [158]. To meet these obstacles, investigators might well consider the design of optimized DL methods that can easily be fixed by accumulating a dataset that contains radiography pictures of Covid19 patients with diverse phases (from Day 1 to 30). Also, there is the possibility of recognizing the Covid Version-1, beta Covid version-2, and delta Covid version-3 through radiography images. If further information becomes available, we can examine photos of the same individuals taken on different days to see how the Covid19 lung infection progresses. Even Covid19 detection uses patients' voice/speech with DL-based RNN LSTM model to find healthy and infected people [43].

Increased risk due to presence of COPD with COVID19: Recent DML experiments made by [19, 21, 24] shows that the existing COPD may increase the severity and mortality rates of COVID19 affected patients. However, ROI + heatmaps detection [19] on same radiograph having chronic diseases along with coronavirus is another challenge.

8.2.2 Future plan

By overcoming the aforementioned hurdles, we will be able to design a custom model in partnership with radiologists for Covid19 detection and classification in conjunction with other

chronic lung disorders. The projected system could be an enterprise application that would be able to access from a remote location using handheld devices with API integration.

Balanced and increased size of dataset: To increase the size of the dataset, balance the dataset, and enhance the training performance of DNN, the maximum authors have used data augmentation [13, 49, 63, 72, 75, 82, 98, 150, 167] technique like GAN, CycleGAN. It was found that with partial data, deep networks struggle at training and deliver a lesser amount of consistency over multi-modal imaging [64]. To overcome the issues with limited dataset and data augmentation, the DeTraC [46] presented operational and robust results for the categorization of Covid19. DeTraC utilizes the benefits of class deconstruction inside CNNs for picture categorization and the partial quantity of training dataset [46]. PCA can reflect deep data vectors onto a relatively low feature space [57] because the lower dimensional images require less computation and time. In contrast, training higher resolution images requires more computation [160]. However, highly correlated features were ignored. Data augmentation helps in class imbalance problems using cropping, flipping, rotation, translation, brightness, contrast, color augmentation, and saturation of samples with the "imgaug" tool [31].

Separation of different types of pneumonia and other lung diseases with Covid-19: Along with the development of the Covid19 diagnosis assistance model for lung image modalities, there is the possibility of verifying the other lung diseases such as tuberculosis, asthma, chronic obstructive pulmonary disease(COPD) [19, 21, 24], chronic bronchitis, emphysema, acute bronchitis, cystic fibrosis, emphysema, pulmonary edema, lung cancer, ARDS, pneumoconiosis, interstitial lung disease, pneumothorax, pleural effusion, mesothelioma, obesity hypoventilation syndrome, etc. and also, searching for the parameters in severity level assessment of Covid19 patients to minimize the severity and mortality rates.

Development of custom model with the large dataset: After understating the various possibilities of detecting Covid19 using variants of DL techniques, still some challenges like, Is the patient infected with Covid19 going to survive or not? Or Finding the side effects of Covid19 disease on the patient's lung region after discharging from the hospital? What is the severity level of Covid19 in the lung region? To overcome the problems with datasets, there is the possibility of building only one central unique dataset that could be accessed globally by many DL researchers and medical practitioners to share radiography images. But there is a chance of keeping in view the secrecy worries of the organizations. We can use a blockchain learning-based technique to overcome such problems [96]. The system must be developed to provide faster results with the highest accuracy within a lesser computational time to achieve higher precision from the pre-trained and custom DL models. We can authentically recognize the asymptotic patients affected lung portion by Covid19 disease by radiography images. YOLO [82] plays a crucial role in real-time object detection from radiograph images and bounding boxes [16].

Imaging modalities: All the studied developed systems utilize single image modalities, either X-ray, CT, or ultrasound. So there is a probability of combining multimodal radiography images to assess Covid19 with other lung diseases, like X-ray and CT, X-ray with ultrasound, and CT with ultrasound [17, 19]. However, it's a cumbersome process to use multimodal imaging. But this may increase the chances of recognizing the lung diseases that were not identified in one image type but may detect the features in others and vice-versa.

Qualification and benchmark performance metrics: A confusion matrix measures an algorithm's effectiveness. When we maintain an unbalanced amount of samples in every class or have more than binary class labels, categorization performance can be incorrect. Preparing a confusion matrix can help us understand whether the classification model is taken correctly or wrong. Table 3 shows that 98% of the researcher's model developed under image modality uses performance metrics like F1-score, sensitivity, specificity, precision, and accuracy. Apart from these measures, the performance of a DL model depends on the data size, the number of epochs, the number of convolution layers, kernel size, pool size, stride, batch size, learning rate, optimizer, and model computation time training, testing, and validation, etc.

Post Covid-19 assessment: To aid decision-making, we must adopt a plan to anticipate the threat of SARS-CoV-2 contamination in the workplace place relying on a study of the working procedures and individual proximity; the chance of infection associated with the type of activity; the participation of third parties in the working processes; and the risk of social aggregation. Also, there is a possibility of classification of alpha, beta, gamma, delta, and IHU, Deltacron mutation of Covid19 using genome sequencing. However, COVID19 variants classification using radiography imaging is another challenge.

9 Limitations of the study

The primary purpose of the whole review study is to highlight the Covid19 detection system, which is based on DL. Even though some of the traits highlighted in the literature are now stressed, these remain indeed limitations that must be considered in upcoming research. We have focused only on that experimentation system with Covid19 detection. Because lack of clear examples and prior information on DNN that emphasizes algebraic and geometric descriptions. We assume that the reader has specific mathematical knowledge. Also, we have tried to discuss the radiography medical imaging domain characteristic related to Covid19 based on lung infection in Section 6, but that knowledge is not enough. In this case, definite medical practitioner exposure is the necessary concern. In Table 3 of the studied pre-trained, hybrid, and custom neural networks for X-ray, CT, and ultrasound images, each author did not disclose the execution time for the developed system. Also, This review work does not provide any source code for developing the Covid19 system. However, this review paper considers only the Covid19 detection system, including pre-trained, hybrid, and custom models, without considering the other types of lung diseases from X-ray, CT, and ultrasound image modes.

10 Conclusion

This paper thoroughly examines the various DL-based pretrained, hybrid, and custom models utilized for recognizing and classifying Covid-19 from X-ray, CT, ultrasound, ECG, and genome sequence modalities. Along with DL, the ML was used to create many remedies for troublesome Covid-19, such as forecasting epidemics, viral propagation monitoring, diagnosis, medication, development of vaccines, and study of drugs. Recently, monkeypox epidemic started in African countries [23], hope this monkyepox shouldn't be another pandemic in near future. We tried to cover most pre-trained, hybrid, and custom networks, datasets used in the

different systems(URL can be used to download the database that helps the researcher to utilize the dataset from Table 1), challenges such as gap analysis with present Covid-19 scenarios, and future work is discussed. The efficient application of DL to manipulate Covid-19 medical images requires considerable time and work and direct relationships among diverse governmental, industrial and academic entities, notwithstanding encouraging outcomes. A range of concerns and challenges have also been identified, including the absence of a global certified dataset, security, regulatory and transparent information, and differences in illnesses among Covid19 versus non-Covid19. It would be an excellent strategy to harness its strengths in ordinary clinical practice in the quest to combat SARS-CoV-2 to integrate computer vision modeling for Covid-19 scanning as a clinical support tool. DL would play a key role in radiographic imagery identification and categorization of Covid-19. It's judicious to note that DL methods with radiography modalities deal only with incomplete facts about the diseased patients. It's not implied in the current study that DL systems can thoroughly substitute the work of radiologists, medical practitioners, or clinicians in diagnosis.

Furthermore, it could also be medically advantageous to employ DL to separate Covid-19 lung infections. For instance, separation filters could direct the doctor's focus to COPDs, pneumonia spots of Covid-19 and can be utilized to quantify lung parenchymal illness accurately. With X-ray and ultrasound for covid-19 detection, CT remains a limited concern due to high cost. X-ray, ECG are frequently modest and cheaper; however more noticeable in CT scans. Heatmap produced for individuals with Covid-19 using lungs gives a hint/assistance to the radiologist to find out the severity and region of lung infected by a coronavirus. In the future, it is expected that radiologists and medical experts with DL experts and data engineers collaborate to make available suitable Covid-19 recognition systems, particularly in the initial phases of the illness, even evaluating the scale of seriousness of the lung contamination. We believe this study is a valuable standard reference. Researchers can conduct several scientific findings throughout the war versus the Covid-19 epidemic regarding DL and computer vision for an alpha, beta, gamma, delta, omicron, IHU, etc. mutations of Covid-19 detection.

Authors contribution Y. H. Bhosale: review and editing, writing – original draft, Conceptualization, Visualization, Formal Analysis, Revision; and K. S. Patnaik: Supervision.

Funding This research did not receive any specific grant from funding agencies in the public, commercial, or not-for-profit sectors.

Declarations

Conflict of interest The authors declare no competing interests.

References

1. 2019nCoVR: RNA Genome Sequence COVID Dataset (2023) January 24, 2023, [Online]. Available: https://bigd.big.ac.cn/ncov
2. Abdani SR, Zulkifley MA, Zulkifley NH (2020) A Lightweight Deep Learning Model for COVID-19 Detection, in 2020 IEEE symposium on Industrial Electronics & Applications (ISIEA), TBD, Malaysia, pp 1–5. https://doi.org/10.1109/ISIEA49364.2020.9188133

3. Abdelminaam DS, Ismail FH, Taha M, Taha A, Houssein EH, Nabil A (2021) CoAID-DEEP: an optimized intelligent framework for automated detecting COVID-19 misleading information on twitter. IEEE Access 9:27840–27867. https://doi.org/10.1109/ACCESS.2021.3058066
4. Acharya UR, Oh SL, Hagiwara Y, Tan JH, Adeli H (2018) Deep convolutional neural network for the automated detection and diagnosis of seizure using eeg signals. Comput Biol Med 100:270–278
5. Ahmed, Pneumonia Sample X-Rays, GitHub, (2019) Accessed on Jun 28 2021 https://www.kaggle.com/ahmedali2019/pneumonia-sample-xrays
6. Ahmed M, Ahmad JJPC, Rodrigues GJ, Din S (2021) A deep learning-based social distance monitoring framework for COVID-19. Sustain Cities Soc 65:102571. https://doi.org/10.1016/j.scs.2020.102571
7. Alakus TB, Turkoglu I (2020) Comparison of deep learning approaches to predict COVID-19 infection. Chaos, Solitons Fractals 140:110120. https://doi.org/10.1016/j.chaos.2020.110120
8. Alizadehsani R, Behjati M, Roshanzamir Z, Hussain S, Abedini N, Hasanzadeh F, Khosravi A, Shoeibi A, Roshanzamir M, Moradnejad P et al. (2020) Risk factors prediction, clinical outcomes, and mortality of covid-19 patients, medRxiv
9. Apostolopoulos D, Aznaouridis SI, Tzani MA (2020) Extracting Possibly Representative COVID-19 Biomarkers from X-ray Images with Deep Learning Approach and Image Data Related to Pulmonary Diseases. J Med Biol Eng 40(3):462–469. https://doi.org/10.1007/s40846-020-00529-4
10. Ardakani A, Kanafi AR, Acharya UR, Khadem N, Mohammadi A (2020) Application of deep learning technique to manage COVID-19 in routine clinical practice using CT images: results of 10 convolutional neural networks. Comput Biol Med 121:103795. https://doi.org/10.1016/j.compbiomed.2020.103795
11. Arntfield R et al. (2020) Development of a deep learning classifier to accurately distinguish COVID-19 from look-a-like pathology on lung ultrasound, Respir Med, preprint. https://doi.org/10.1101/2020.10.13.20212258
12. Aslan MF, Unlersen MF, Sabanci K, Durdu A (2021) CNN-based transfer learning–BiLSTM network: a novel approach for COVID-19 infection detection. Appl Soft Comput 98:106912. https://doi.org/10.1016/j.asoc.2020.106912
13. Bassi PRAS, Attux R (2022) A deep convolutional neural network for COVID-19 detection using chest X-rays, Res Biomed Eng 38:139–148. https://doi.org/10.1007/s42600-021-00132-9
14. Bhattacharyya A, Bhaik D, Kumar S, Thakur P, Sharma R, Pachori RB (2022) A deep learning based approach for automatic detection of COVID-19 cases using chest X-ray images, Biomed Signal Process Control, Volume 71, Part B, 103,182, https://doi.org/10.1016/j.bspc.2021.103182
15. Bhoi SK, Jena KK, Mohapatra D, Singh M, Kumar R, Long HV (2021) Communicable disease pandemic: a simulation model based on community transmission and social distancing. Soft Comput. https://doi.org/10.1007/s00500-021-06168-4
16. Bhosale YH (2020) Digitization Of Households With Population Using Cluster And List Sampling Frame In Aerial Images", ISSN (Online) 2456–3293 www.oaijse.com, vol 5.,issue 2, pp 22–26
17. Bhosale YH, Patnaik KS (2022) Graph and capsule convolutional neural network based classification of lung Cancer, pneumonia, COVID-19 using lung CT and ultrasound radiography imaging, 2022 8th international conference on signal processing and communication (ICSC), Noida, India, pp 381–387, https://doi.org/10.1109/ICSC56524.2022.10009568
18. Bhosale YH, Patnaik KS (2022) Application of deep learning techniques in diagnosis of Covid-19 (coronavirus): a systematic review. Neural Process Lett:1–53. https://doi.org/10.1007/s11063-022-11023-0
19. Bhosale YH, Patnaik KS (2023) PulDi-COVID: chronic obstructive pulmonary (lung) diseases with COVID-19 classification using ensemble deep convolutional neural network from chest X-ray images to minimize severity and mortality rates. Biomed Signal Process Control 81:104445. https://doi.org/10.1016/j.bspc.2022.104445
20. Bhosale YH, Patnaik KS (n.d.) ECG-CCNet: Cardiovascular(Cardiac) and COVID-19 Disease Classification Using Deep Convolutional Neural Network Learning Pipeline Approaches From Electrocardiography(ECG)- A Study, 2022 IEEE Silchar Subsection Conference (IEEE-SILCON), pp doi
21. Bhosale YH, Sridhar Patnaik K (2022) IoT Deployable Lightweight Deep Learning Application For COVID-19 Detection With Lung Diseases Using RaspberryPi, 2022 International Conference on IoT and Blockchain Technology (ICIBT), Ranchi, India, pp 1–6, https://doi.org/10.1109/ICIBT52874.2022.9807725
22. Bhosale YH, Zanwar S, Ahmed Z, Nakrani M, Bhuyar D, Shinde U (2022) Deep Convolutional Neural Network Based Covid-19 Classification From Radiology X-Ray Images For IoT Enabled Devices, 2022 8th international conference on advanced computing and communication systems (ICACCS), Coimbatore, India, pp 1398–1402, https://doi.org/10.1109/ICACCS54159.2022.9785113
23. Bhosale YH, Zanwar SR, Jadhav AT, Ahmed Z, Gaikwad VS, Gandle KS (2022) Human Monkeypox 2022 Virus: Machine Learning Prediction Model, Outbreak Forecasting, Visualization with Time-Series

Exploratory Data Analysis, 2022 13th International Conference on Computing Communication and Networking Technologies (ICCCNT), Kharagpur, India, pp 1–6, https://doi.org/10.1109/ICCCNT54827.2022.9984237.
24. Bhosale YH, Singh P, Patnaik KS (2023) COVID-19 and associated lung disease classification using deep learning. In: international conference on innovative computing and communications. Lecture notes in networks and systems, vol 492. Springer, Singapore. https://doi.org/10.1007/978-981-19-3679-1_22
25. Biorxiv CT Dataset (2021) Accessed on Jun 16, 2021, https://www.biorxiv.org/
26. Born J et al (2021) Accelerating Detection of Lung Pathologies with Explainable Ultrasound Image Analysis. Appl Sci 11(2):672. https://doi.org/10.3390/app11020672
27. Born J et al. (2021) POCOVID-Net: Automatic Detection of COVID-19 From a New Lung Ultrasound Imaging Dataset (POCUS), arXiv:2004.12084 [cs, eess], Jan. 2021, Accessed on Jul 06, 2021. [Online]. Available: http://arxiv.org/abs/2004.12084
28. Born et al. (2021) POCOVID-Net data set. Accessed on Jun 26 2021 https://github.com/jannisborn/covid19_ultrasound/tree/master/data
29. Chen J (2020) Deep learning-based model for detecting 2019 novel coronavirus pneumonia on high-resolution computed tomography, Sci Rep, p 11
30. Chest x-ray images from the Indiana University hospital (n.d.) Accessed on Jun 262,021 https://openi.nlm.nih.gov/
31. Common augmentation sequence: imgaug (2021) Accessed on 14 Oct. 2021 https://imgaug.readthedocs.io/en/latest/source/examples_basics.html
32. Covid 19 RT PCR Test in Cochin (2021) Accessed on 14 Oct. 2021 https://www.metropolisindia.com/parameter/cochin/covid-19-rt-pcr-test#:~:text=How%20long%20will%20it%20take,reports%20delivered%20within%2048*%20 hours
33. COVID-19 chest X-ray Database (2021) Accessed on Jun 14, 2021, https://github.com/agchung
34. COVID-19 CT Lung and Infection Segmentation Dataset (2021) Accessed on Jun 21, 2021, https://zenodo.org/record/3757476#.YNBXMt3hXIU
35. COVID-19 CT Segmentation Dataset (2021) Accessed on Jun 18, 2021, http://medicalsegmentation.com/covid19/
36. Covid-19 Database (2021) Accessed on Jun 14, 2021, https://radiopaedia.org/
37. COVID-19 database SIRM (2021) Accessed on Jun 14, 2021, https://www.sirm.org/en/category/articles/covid-19-database/
38. COVID-19 Radiography Database: Chest X-ray (2021) Accessed on Jun 17, 2021, https://www.kaggle.com/tawsifurrahman/covid19-radiography-database
39. COVID-19 X-rays and CT snapshots of CONVID-19 patients Kaggle dataset (2021) Accessed on Jun 22, 2021, https://www.kaggle.com/andrewmvd/convid19-x-rays
40. COVID-CT-Dataset: a CT scan dataset about COVID-19 (2021) Accessed on Jun 16, 2021, https://github.com/UCSD-AI4H/COVID-CT
41. D'Agostino MA (2010) Ultrasound imaging in spondyloarthropath ies. Best Practice Res Clin Rheumatol 24(5):693–700. https://doi.org/10.1016/j.berh.2010.05.003
42. Dataset tuberculosis (2023) Accessed: January 24, 2023, [Online]. Available: http://www.kaggle.com/kmader/pulmonary-chest-xray-abnormalities
43. Desai SB, Pareek A, Lungren MP (2020) Deep learning and its role in COVID-19 medical imaging. Intell Based Med 3–4:100013. https://doi.org/10.1016/j.ibmed.2020.100013
44. Distelmaier F, Göbel U, Vandemeulebroecke N, Mayatepek E, Rosenbaum T, Laws H-J (2007) Secondary pseudotumor cerebri in pediatric oncology and hematology: An unpredictable condition of varying etiology. Pediatr. Blood Cancer 49:1029–1033. https://doi.org/10.1002/pbc.20783
45. Dong D et al (2021) The Role of Imaging in the Detection and Management of COVID-19: A Review. IEEE Rev. Biomed. Eng. 14:16–29. https://doi.org/10.1109/RBME.2020.2990959
46. El Asnaoui K, Chawki Y (2020) Using X-ray images and deep learning for automated detection of coronavirus disease, J Biomol Struct Dyn, pp 1–12, https://doi.org/10.1080/07391102.2020.1767212.
47. Esteva A, Kuprel B, Novoa RA, Ko J, Swetter SM, Blau HM, Thrun S (2017) Dermatologist-level classification of skin cancer with deep neural networks. Nature 542(7639):115–118
48. Figure 1 covid-19 clinical cases (2021) Accessed on Jun 17, 2021, https://www.figure1.com/covid-19-clinical-cases
49. Fontanellaz M, Ebner L, Huber A, Peters A, Löbelenz L, Hourscht C, Klaus J, Munz J, Ruder T, Drakopoulos D, Sieron D, Primetis E, Heverhagen JT, Mougiakakou S, Christe A (2021) A deep-learning diagnostic support system for the detection of COVID-19 using chest radiographs: a multireader validation study. Investig Radiol 56(6):348–356. https://doi.org/10.1097/RLI.0000000000000748

50. Ghassemi N, Shoeibi A, Rouhani M, Hosseini-Nejad H (2019) Epileptic seizures detection in eeg signals using tqwt and ensemble learning, in 2019 9th International Conference on Computer and Knowledge Engineering (ICCKE). IEEE, pp 403–408
51. Ghassemi N, Shoeibi A, Rouhani M (2020) Deep neural network with generative adversarial networks pre-training for brain tumor classification based on mr images. Biomedical Signal Processing and Control 57: 101678
52. Github arthursdays HKBU-HPML-COVID-19 CT dataset (n.d.) Accessed on June 222,021 https://github.com/arthursdays/HKBU_HPML_COVID-19
53. Github: BorgwardtLab Dataset (n.d.) Accessed on Jun 282,021 https://github.com/BorgwardtLab/covid19_ultrasound
54. GitHub: covid-chestxray-dataset (2021) Accessed on Jun 14, 2021, https://github.com/ieee8023/covid-chestxray-dataset
55. Github: muhammedtalo X-Ray (2021) Accessed on Jun 18, 2021, https://github.com/muhammedtalo/COVID-19/tree/master/X-Ray%20Image%20DataSet
56. GitHub: SARS-COV-2 Ct-Scan Dataset (2021) Accessed on Jun 15, 2021, https://www.kaggle.com/plameneduardo/sarscov2-ctscan-dataset
57. Gozes O, Frid-Adar M, Sagie N, Zhang H, Ji W, Greenspan H (2020) Coronavirus Detection and Analysis on Chest CT with Deep Learning, arXiv:2004.02640 [cs, eess], Accessed: Jun. 10, 2021. [Online]. Available: http://arxiv.org/abs/2004.02640
58. Gudla SPK, Bhoi SK (2022) MLP Deep Learning-based DDoS Attack Detection Framework for Fog Computing. In: Rout RR, Ghosh SK, Jana PK, Tripathy AK, Sahoo JP, Li KC (eds) Advances in Distributed Computing and Machine Learning. Lecture Notes in Networks and Systems, vol 427. Springer, Singapore. https://doi.org/10.1007/978-981-19-1018-0_3
59. Han Z, Wei B, Hong Y, Li T, Cong J, Zhu X, Wei H, Zhang W (2020) Accurate screening of COVID-19 using attention-based deep 3D multiple instance learning. IEEE Trans Med Imaging 39(8):2584–2594. https://doi.org/10.1109/TMI.2020.2996256
60. Harapan H, Itoh N, Yufika A, Winardi W, Keam S, te H, Megawati D, Hayati Z, Wagner AL, Mudatsir M (2020) Coronavirus disease 2019 (COVID-19): a literature review. J Infect Public Health 13(5):667–673. https://doi.org/10.1016/j.jiph.2020.03.019
61. Harikrishnan N, Pranay S, Nagaraj N (2022) Classification of SARS-CoV-2 viral genome sequences using Neurochaos Learning. Med Biol Eng Comput 60:2245–2255. https://doi.org/10.1007/s11517-022-02591-3
62. He X. et al. (2020) Benchmarking Deep Learning Models and Automated Model Design for COVID-19 Detection with Chest CT Scans, Epidemiology, preprint. https://doi.org/10.1101/2020.06.08.20125963.
63. Hernández Santa Cruz JF (2021) An ensemble approach for multi-stage transfer learning models for COVID-19 detection from chest CT scans. Int-Based Med 5:100027. https://doi.org/10.1016/j.ibmed.2021.100027
64. Horry MJ, Chakraborty S, Paul M, Ulhaq A, Pradhan B, Saha M, Shukla N (2020) COVID-19 detection through transfer learning using multimodal imaging data. IEEE Access 8:149808–149824. https://doi.org/10.1109/ACCESS.2020.3016780
65. How AarogyaSetu knows about Covid-19 positive status (2021) Accessed on 10 Oct. 2021 https://www.aarogyasetu.gov.in/
66. Hussain E., M. Hasan, M. A. Rahman, I. Lee, T. Tamanna, and M. Z. Parvez, CoroDet: A deep learning based classification for COVID-19 detection using chest X-ray images, Chaos, Solitons Fractals, 142: 110495, 2021, https://doi.org/10.1016/j.chaos.2020.110495
67. IEEEDataport: CCAP-CT data sets from multi-centre hospitals included five categories (2021) Accessed on Jun 21, 2021, https://ieee-dataport.org/documents/ccap
68. Ilyas M, Rehman H, Nait-ali A (2020) Detection of Covid-19 From Chest X-ray Images Using Artificial Intelligence: An Early Review, arXiv:2004.05436 [cs, eess], Accessed: Jun. 10, 2021. [Online]. Available: http://arxiv.org/abs/2004.05436
69. Iosifidis C, Agha R (2020) World health organization declares global emergency: A review of the 2019 novel coronavirus (covid-19), Int J Surg
70. Irmak E (2020) A Novel Deep Convolutional Neural Network Model for COVID-19 Disease Detection, in 2020 Medical technologies congress (TIPTEKNO), Antalya, Turkey, pp 1–4. https://doi.org/10.1109/TIPTEKNO50054.2020.9299286
71. Irmak E (2022) COVID-19 disease diagnosis from paper-based ECG trace image data using a novel convolutional neural network model. Phys Eng Sci Med **45**:167–179. https://doi.org/10.1007/s13246-022-01102-w
72. Islam Z, Islam M, Asraf A (2020) A combined deep CNN-LSTM network for the detection of novel coronavirus (COVID-19) using X-ray images. Inf Med Unlocked 20:100412. https://doi.org/10.1016/j.imu.2020.100412

73. Islam M, Karray F, Alhajj R, Zeng J (2021) A Review on Deep Learning Techniques for the Diagnosis of Novel Coronavirus (COVID-19). IEEE Access 9:30551–30572. https://doi.org/10.1109/ACCESS.2021.3058537
74. Italian COVID-19 Lung Ultrasound DataBase (ICLUS-DB) (2021) Accessed on Jun 30 2021 https://iclus-web.bluetensor.ai
75. Jain G, Mittal D, Thakur D, Mittal MK (2020) A deep learning approach to detect Covid-19 coronavirus with X-ray images. Biocybern Biomed Eng 40(4):1391–1405. https://doi.org/10.1016/j.bbe.2020.08.008
76. Jain R, Gupta M, Taneja S, Jude Hemanth D (2021) Deep learning based detection and analysis of COVID-19 on chest X-ray images. Appl Intell 51:1690–1700. https://doi.org/10.1007/s10489-020-01902-1
77. Jaiswal, N Gianchandani, D Singh, VK, Kaur M (2020) Classification of the COVID-19 infected patients using DenseNet201 based deep transfer learning, J Biomol Struct Dyn, pp 1–8, https://doi.org/10.1080/07391102.2020.1788642.
78. Jena KK, Bhoi SK, Nayak SR, Mallick C (2021) Machine Learning-Based Virus Type Classification Using Transmission Electron Microscopy Virus Images, https://doi.org/10.1002/9781119786122.ch1
79. Jena KK, Bhoi SK, Nayak SR, Pattanaik CR (2022) Machine learning-based classification: an analysis based on COVID-19 transmission electron microscopy images. International Journal of Computer Applications in Technology 66, No. 3–4:350–361. https://doi.org/10.1504/IJCAT.2021.120462
80. Jena KK, Bhoi SK, Prasad M, Puthal D (2022) A fuzzy rule-based efficient hospital bed management approach for coronavirus disease-19 infected patients. Neural Comput Applic 34:11361–11382. https://doi.org/10.1007/s00521-021-05719-y
81. Jiang Y, Chen H, Loew M, Ko H (2021) COVID-19 CT image synthesis with a conditional generative adversarial network. IEEE J Biomed Health Inform 25(2):441–452. https://doi.org/10.1109/JBHI.2020.3042523
82. Joshi RC, Yadav S, Pathak VK, Malhotra HS, Khokhar HVS, Parihar A, Kohli N, Himanshu D, Garg RK, Bhatt MLB, Kumar R, Singh NP, Sardana V, Burget R, Alippi C, Travieso-Gonzalez CM, Dutta MK (2021) A deep learning-based COVID-19 automatic diagnostic framework using chest X-ray images. Biocybern Biomed Eng 41(1):239–254. https://doi.org/10.1016/j.bbe.2021.01.002
83. Kaggle chest x-ray repository (2021) Accessed on Jun 14, 2021, https://www.kaggle.com/paultimothymooney/chest-xray-pneumonia
84. kaggle COVID-19 chest XRay: COVID-19 image data collection (Bachrr) (2021) Accessed on June 22 2021 https://www.kaggle.com/bachrr/covid-chest-xray
85. Kalane P, Patil S, Patil BP, Sharma DP (2021) Automatic detection of COVID-19 disease using U-net architecture based fully convolutional network. Biomed Signal Process Control 67:102518. https://doi.org/10.1016/j.bspc.2021.102518
86. Karhan Z, Akal F (2020) Covid-19 Classification Using Deep Learning in Chest X-Ray Images, in 2020 Medical technologies congress (TIPTEKNO), Antalya, Turkey, pp 1–4. https://doi.org/10.1109/TIPTEKNO50054.2020.9299315
87. Karthik R, Menaka R, Hariharan M (2021) Learning distinctive filters for COVID-19 detection from chest X-ray using shuffled residual CNN. Appl Soft Comput 99:106744. https://doi.org/10.1016/j.asoc.2020.106744
88. Kastelein John J.P., Eric de Groot, Ultrasound imaging techniques for the evaluation of cardiovascular therapies, European Heart Journal, Volume 29, Issue 7, April 2008, Pages 849–858, https://doi.org/10.1093/eurheartj/ehn070
89. Kermany D et al. (2021) Large Dataset of Labeled Optical Coherence Tomography (OCT) and Chest X-Ray Images. Accessed on Jun 24 2021 https://data.mendeley.com/datasets/rscbjbr9sj/3
90. Khan I, Shah JL, Bhat MM (2020) CoroNet: a deep neural network for detection and diagnosis of COVID-19 from chest x-ray images. Comput Methods Prog Biomed 196:105581. https://doi.org/10.1016/j.cmpb.2020.105581
91. Khan AH et al (2021) ECG Images dataset of Cardiac and COVID-19 Patients. Data Brief 34:106–762 ISSN 2352–3409
92. Khan E, Rehman MZU, Ahmed F, Alfouzan FA, Alzahrani NM, Ahmad J (2022) Chest X-ray Classification for the Detection of COVID-19 Using Deep Learning Techniques. Sensors. 22(3):1211. https://doi.org/10.3390/s22031211
93. Konar D, Panigrahi BK, Bhattacharyya S, Dey N, Jiang R (2021) Auto-diagnosis of COVID-19 using lung CT images with semi-supervised shallow learning network. IEEE Access 9:28716–28728. https://doi.org/10.1109/ACCESS.2021.3058854
94. Kroft LJ, van der Velden L, Giròn IH, Roelofs JJ, de Roos A, Geleijns J (2019) Added value of ultra–low-dose computed tomography, dose equivalent to chest x-ray radiography, for diagnosing chest pathology. Journal of thoracic imaging 34(3):179

95. Lencioni R, Piscaglia F, Bolondi L (2008) Contrast-enhanced ultrasound in the diagnosis of hepatocellular carcinoma. Journal of Hepatology 48(5):848–857, ISSN 0168–8278. https://doi.org/10.1016/j.jhep.2008.02.005
96. Li L, Qin L, Xu Z, Yin Y, Wang X, Kong B, Bai J, Lu Y, Fang Z, Song Q, Cao K, Liu D, Wang G, Xu Q, Fang X, Zhang S, Xia J, Xia J (2020) Using artificial intelligence to detect COVID-19 and community-acquired pneumonia based on pulmonary CT: evaluation of the diagnostic accuracy. Radiology 296(2): E65–E71. https://doi.org/10.1148/radiol.2020200905
97. Liu X, He J, Song L, Liu S, Srivastava G (2021, Article No.: 102) Medical Image Classification based on an Adaptive Size Deep Learning Model. ACM Transactions on Multimedia Computing, Communications, and Applications 17(3):1–18. https://doi.org/10.1145/3465220
98. Loey M, Manogaran G, Khalifa NEM (2020) A deep transfer learning model with classical data augmentation and CGAN to detect COVID-19 from chest CT radiography digital images, Neural Comput Applic, https://doi.org/10.1007/s00521-020-05437-x.
99. Loey M, Manogaran G, Taha MHN, Khalifa NEM (Jan. 2021) A hybrid deep transfer learning model with machine learning methods for face mask detection in the era of the COVID-19 pandemic. Measurement 167:108288. https://doi.org/10.1016/j.measurement.2020.108288
100. Luz E, Silva P, Silva R, Silva L, Guimarães J, Miozzo G, Moreira G, Menotti D (2022) Towards an effective and efficient deep learning model for COVID-19 patterns detection in X-ray images. Res. Biomed. Eng. 38:149–162. https://doi.org/10.1007/s42600-021-00151-6
101. Majeed T, Rashid R, Ali D., Asaad A (2020) Covid-19 detection using CNN transfer learning from X-ray Images. Medrxiv (2020): 2020-05
102. Mazurowski MA, Buda M, Saha A, Bashir MR (2019) Deep learning in radiology: An overview of the concepts and a survey of the state of the art with focus on mri. J Magnet Reson Imaging 49(4):939–954
103. Medhi K, Jamil, Hussain I (2020) Automatic Detection of COVID-19 Infection from Chest X-ray using Deep Learning, Health Informatics, preprint. https://doi.org/10.1101/2020.05.10.20097063
104. Medrxiv CT Dataset (2021) Accessed on 16 Jun 16, 2021, https://www.medrxiv.org/
105. Ministry HFW COVID Report (2022) Accessed on: January 27, 2022: [Online]. Available: https://www.mohfw.gov.in/
106. Mohammadpoor M, Shoeibi A, Zare H, Shojaee H (2016) A hierarchical classification method for breast tumor detection. Iran J Med Phys 13(4):261–268
107. Mostafiz R, Uddin MS, Alam NA, Reza M, Rahman MM (2020) Covid-19 detection in chest X-ray through random forest classifier using a hybridization of deep CNN and DWT optimized features, J King Saud Univ Comput Inf Sci, p S1319157820306182, https://doi.org/10.1016/j.jksuci.2020.12.010.
108. Muhammad G, Shamim Hossain M (2021) COVID-19 and non-COVID-19 classification using multi-layers fusion from lung ultrasound images. Inf Fus 72:80–88. https://doi.org/10.1016/j.inffus.2021.02.013
109. Mukherjee H, Ghosh S, Dhar A, Obaidullah SM, Santosh KC, Roy K (2021) Shallow convolutional neural network for COVID-19 outbreak screening using chest X-rays, Cogn Comput, https://doi.org/10.1007/s12559-020-09775-9
110. Narayan Das N, Kumar N., Kaur M, Kumar V, Singh D (2020) Automated Deep Transfer Learning-Based Approach for Detection of COVID-19 Infection in Chest X-rays, IRBM, p S1959031820301172, https://doi.org/10.1016/j.irbm.2020.07.001.
111. Narin, CK, Pamuk Z (2021) Automatic detection of coronavirus disease (COVID-19) using X-ray images and deep convolutional neural networks, Pattern Anal Applic, https://doi.org/10.1007/s10044-021-00984-y
112. Nayak SR, Nayak DR, Sinha U, Arora V, Pachori RB (2021) Application of deep learning techniques for detection of COVID-19 cases using chest X-ray images: a comprehensive study. Biomed Signal Process Control 64:102365. https://doi.org/10.1016/j.bspc.2020.102365
113. Nazari K., M. J. Ebadi, and K. Berahmand, Diagnosis of Alternaria disease and leafminer pest on tomato leaves using image processing techniques, J. Sci. Food Agric., 102(15):6907–6920, Dec. 2022, https://doi.org/10.1002/JSFA.12052.10.1002/jsfa.12052
114. Negin medical center [Online] (2021) Accessed on Jun 18, 2021, https://github.com/mr7495/COVID-CTset
115. Ni Q, Sun ZY, Qi L, Chen W, Yang Y, Wang L, Zhang X, Yang L, Fang Y, Xing Z, Zhou Z, Yu Y, Lu GM, Zhang LJ (2020) A deep learning approach to characterize 2019 coronavirus disease (COVID-19) pneumonia in chest CT images. Eur Radiol 30(12):6517–6527. https://doi.org/10.1007/s00330-020-07044-9
116. NIH chest X-rays, Kaggle (2021) Accessed on Jun 14, 2021, https://www.kaggle.com/nih-chest-xrays/data?select=Data_Entry_2017.csv
117. Nithya A., Ahilan Appathurai, N. Venkatadri, D.R. Ramji, C. Anna Palagan, Kidney disease detection and segmentation using artificial neural network and multi-kernel k-means clustering for ultrasound images, Meas, Volume 149, 2020, 106,952, https://doi.org/10.1016/j.measurement.2019.106952

118. Nour M, Cömert Z, Polat K (Dec. 2020) A novel medical diagnosis model for COVID-19 infection detection based on deep features and Bayesian optimization. Appl Soft Comput 97:106580. https://doi.org/10.1016/j.asoc.2020.106580
119. Orioli L., M. P Hermans, J.-P. Thissen, D. Maiter, B. Vandeleene, and J.-C. Yombi (2020) Covid-19 in diabetic patients: related risks and specifics of management, in Annales D'endocrinologie. Elsevier
120. Ouchicha C., O. Ammor, and M. Meknassi, CVDNet: A novel deep learning architecture for detection of coronavirus (Covid-19) from chest x-ray images, Chaos, Solitons Fractals, 140:110245, Nov. 2020, https://doi.org/10.1016/j.chaos.2020.110245.
121. Ozcan T (2020) A Deep Learning Framework for Coronavirus Disease (COVID-19) Detection in X-Ray Images, In Review, preprint. https://doi.org/10.21203/rs.3.rs-26500/v1.
122. Ozturk T, Talo M, Yildirim EA, Baloglu UB, Yildirim O, Rajendra Acharya U (2020) Automated detection of COVID-19 cases using deep neural networks with X-ray images. Comput Biol Med 121: 103792. https://doi.org/10.1016/j.compbiomed.2020.103792
123. PACIFIC: RNA Genome SEQUENCE DATASET (2023) January 25, 2023, [Online]. Available: https://github.com/pacific-2020/pacific/ and https://doi.org/10.1038/s41598-021-82,043-4
124. Paluru N, Dayal A, Jenssen HB, Sakinis T, Cenkeramaddi LR, Prakash J, Yalavarthy PK (2021) Anam-net: anamorphic depth embedding-based lightweight CNN for segmentation of anomalies in COVID-19 chest CT images. IEEE Trans Neural Netw Learn Syst 32(3):932–946. https://doi.org/10.1109/TNNLS.2021.3054746
125. Pandit MK, Banday SA, Naaz R, Chishti MA (2021) Automatic detection of COVID-19 from chest radiographs using deep learning. Radiography 27(2):483–489. https://doi.org/10.1016/j.radi.2020.10.018
126. Panwar H, Gupta PK, Siddiqui MK, Morales-Menendez R, Singh V (2020) Application of deep learning for fast detection of COVID-19 in X-Rays using nCOVnet. Chaos, Solitons Fractals 138:109944. https://doi.org/10.1016/j.chaos.2020.109944
127. Ping An Good Doctor, showcases AI-powered, unstaffed clinics (2021) Accessed on 11 Oct. 2021 https://www.mobihealthnews.com/news/asia/ping-good-doctor-showcases-ai-powered-unstaffed-clinics
128. Purohit K, Kesarwani A, Kisku DR, Dalui M (n.d.) COVID-19 Detection on Chest X-Ray and CT Scan Images Using Multi-image Augmented Deep Learning Model, bioRxiv 2020.07.15.205567; https://doi.org/10.1101/2020.07.15.205567
129. Radiological Society of North America. RSNA Pneumonia Detection Challenge (2021) Accessed on Jun 17, 2021, https://www.kaggle.com/c/rsna-pneumonia-detection-challenge/
130. Rafi TH (2020) An ensemble deep transfer-learning approach to identify COVID-19 cases from chest X-ray images, in 2020 IEEE Conference on Computational Intelligence in Bioinformatics and Computational Biology (CIBCB), Via del Mar, Chile, pp 1–5. https://doi.org/10.1109/CIBCB48159.2020.9277695.
131. Rahimzadeh M, Attar A (2020) A modified deep convolutional neural network for detecting COVID-19 and pneumonia from chest X-ray images based on the concatenation of Xception and ResNet50V2. Inf Med Unlocked 19:100360. https://doi.org/10.1016/j.imu.2020.100360
132. Rahimzadeh M, Attar A, Sakhaei SM (2020) A Fully Automated Deep Learning-based Network For Detecting COVID-19 from a New And Large Lung CT Scan Dataset, p 19
133. Rajaraman S, Siegelman J, Alderson PO, Folio LS, Folio LR, Antani SK (2020) Iteratively pruned deep learning ensembles for COVID-19 detection in chest X-rays. IEEE Access 8:115041–115050. https://doi.org/10.1109/ACCESS.2020.3003810
134. Worldmeters: COVID-19 Updates: Real-time database and live updates of Covid-19 cases (n.d.) https://www.worldometers.info/coronavirus/64
135. Islam R, Nahiduzzaman (2022) Complex features extraction with deep learning model for the detection of COVID19 from CT scan images using ensemble based machine learning approach. Expert Systems with Applications 195:116,554. https://doi.org/10.1016/j.eswa.2022.116554
136. Rojas-Azabache C, Vilca-Janampa K, Guerrero-Huayta R, Núñez-Fernández D (2021) Detection of COVID-19 Disease using Deep Neural Networks with Ultrasound Imaging, arXiv:2104.01509 [cs, eess] , Apr. 2021, Accessed: Jul. 06, 2021. [Online]. Available: http://arxiv.org/abs/2104.01509
137. Rostami M, Berahmand K, Nasiri E, Forouzandeh S (2021) Review of swarm intelligence-based feature selection methods. Eng Appl Artif Intell 100:104–210. https://doi.org/10.1016/j.engappai.2021.104210
138. Rostami M, Forouzandeh S, Berahmand K, Soltani M, Shahsavari M, Oussalah M (2022) Gene selection for microarray data classification via multi-objective graph theoretic-based method. Artificial Intelligence in Medicine 123:102,228. https://doi.org/10.1016/j.artmed.2021.102228
139. Roy S, Menapace W, Oei S, Luijten B, Fini E, Saltori C, Huijben I, Chennakeshava N, Mento F, Sentelli A, Peschiera E, Trevisan R, Maschietto G, Torri E, Inchingolo R, Smargiassi A, Soldati G, Rota P, Passerini A, … Demi L (Aug. 2020) Deep learning for classification and localization of COVID-19 markers in point-of-care lung ultrasound. IEEE Trans Med Imaging 39(8):2676–2687. https://doi.org/10.1109/TMI.2020.2994459

140. Rubin GD, CJ Ryerson, LB, Haramati N, Sverzellati JP, Kanne S, Raoof NW, Schluger A, Volpi JJ, Yim IB,. Martin et al. (2020) The role of chest imaging in patient management during the covid-19 pandemic: a multinational consensus statement from the fleischner society, Chest
141. Saberi-Movahed F, Mohammadifard M, Mehrpooya A, Rezaei-Ravari M, Berahmand K, Rostami M, Karami S, Najafzadeh M, Hajinezhad D, Jamshidi M, Abedi F, Mohammadifard M, Farbod E, Safavi F, Dorvash M, Vahedi S, Eftekhari M, Saberi-Movahed F, Tavassoly I (2021) Decoding Clinical Biomarker Space of COVID-19: Exploring Matrix Factorization-based Feature Selection Methods, medRxiv, p 2021.07.07.21259699, https://doi.org/10.1101/2021.07.07.21259699.
142. Saeedi, MS, Maghsoudi A (n.d.) A Novel and Reliable Deep Learning Web-Based Tool to Detect COVID-19 Infection from Chest CT-Scan, p 9
143. Saiz F, Barandiaran I (2020) COVID-19 Detection in Chest X-ray Images using a Deep Learning Approach. IJIMAI 6(2):4. https://doi.org/10.9781/ijimai.2020.04.003
144. Salman FM, Abu-Naser SS, Alajrami E, Abu-Nasser BS, Ashqar BAM (2020) COVID-19 Detection using Artificial Intelligence, 4(3):8
145. Sedik A, Hammad M, Abd FE, El-Samie BB, Gupta & Ahmed A. Abd El-Latif (2022) Efficient deep learning approach for augmented detection of Coronavirus disease. Neural Comput & Applic 34:11423–11440. https://doi.org/10.1007/s00521-020-05410-8
146. Self WH, Courtney DM, McNaughton CD, Wunderink RG, Kline JA (2013) High discordance of chest x-ray and computed tomography for detection of pulmonary opacities in ed patients: implications for diagnosing pneumonia. The American journal of emergency medicine 31(2):401–405
147. Sethy PK, Behera SK, Ratha PK, Biswas P (2020) Detection of coronavirus Disease (COVID-19) based on Deep Features and Support Vector Machine. Int J Math, Eng, Manag Sci 5(4):643–651. https://doi.org/10.33889/IJMEMS.2020.5.4.052
148. Sevi M, Aydin I (2020) COVID-19 Detection Using Deep Learning Methods, in 2020 International conference on data analytics for business and industry: way towards a sustainable economy (ICDABI), Sakheer, Bahrain, pp 1–6. https://doi.org/10.1109/ICDABI51230.2020.9325626.
149. SIIM-FISABIO-RSNA COVID-19 Detection Challenge (2023) Accessed On January 24, 2023. [Online]. Available: https://www.kaggle.com/c/siim-covid19-detection
150. Silva P, Luz E, Silva G, Moreira G, Silva R, Lucio D, Menotti D (2020) COVID-19 detection in CT images with deep learning: a voting-based scheme and cross-datasets analysis. Inf Med Unlocked 20:100427. https://doi.org/10.1016/j.imu.2020.100427
151. Singh OP, Vallejo M, El-Badawy IM, Aysha A, Madhanagopal J, Faudzi AAM (2021) Classifcation of SARS-CoV-2 and nonSARS-CoV-2 using machine learning algorithms. Comput Biol Med 136:104650
152. Song L, Liu X, Chen S, Liu S, Liu X, Muhammad K, Siddhartha Bhattacharyya A (2022) Deep fuzzy model for diagnosis of COVID-19 from CT images. Appl Soft Comput 122:108–883, ISSN 1568–4946. https://doi.org/10.1016/j.asoc.2022.108883
153. Song W, Horton J, Howell J (2023) China Covid How many cases and deaths are there?, Accessed on January 27, 2023, [Online] https://www.bbc.com/news/59882774
154. Steinl DC, Kaufmann BA (2015) Ultrasound Imaging for Risk Assessment in Atherosclerosis. Int. J. Mol. Sci. 16:9749–9769. https://doi.org/10.3390/ijms16059749
155. Subramanian N, Elharrouss O, Al-Maadeed S, Chowdhury M (2022) A review of deep learning-based detection methods for COVID-19. Comput Biol Med 143(105):233. https://doi.org/10.1016/j.compbiomed.2022.105233
156. Talo M, Yildirim O, Baloglu UB, Aydin G, Acharya UR (2019) Convolutional neural networks for multi-class brain disease detection using mri images. Comput Med Imaging Graph 78:101673
157. The cancer imaging archive (TCIA) (2021) Accessed on Jun 14, 2021, https://www.cancerimagingarchive.net/
158. Toğaçar M, Ergen B, Cömert Z (2020) COVID-19 detection using deep learning models to exploit social mimic optimization and structured chest X-ray images using fuzzy color and stacking approaches. Comput Biol Med 121:103805. https://doi.org/10.1016/j.compbiomed.2020.103805
159. Understanding ML Confusion Matrix for performance evaluation (2021) Accessed on 16 Oct. 2021 https://towardsdatascience.com/understanding-confusion-matrix-a9ad42dcfd62
160. Verma P, Tripathi V, Pant B (2021) Comparison of different optimizers implemented on the deep learning architectures for COVID-19 classification, Materials Today: Proceedings, p S2214785321013316, https://doi.org/10.1016/j.matpr.2021.02.244
161. Villanueva F, Wagner W (2008) Ultrasound molecular imaging of cardiovascular disease. Nat Rev. Cardiol 5:S26–S32. https://doi.org/10.1038/ncpcardio1246
162. W. C. D. C. Dashboard (Online) (2023) Accessed on 27 January 2023 https://covid19.who.int
163. Wang Z, Tang K (2020) Combating COVID-19: health equity matters. Nat Med 26(4):458–458. https://doi.org/10.1038/s41591-020-0823-6

164. Wang X, Deng X, Fu Q, Zhou Q, Feng J, Ma H, Liu W, Zheng C (2020) A weakly-supervised framework for COVID-19 classification and lesion localization from chest CT. IEEE Trans Med Imaging 39(8):2615–2625. https://doi.org/10.1109/TMI.2020.2995965
165. Wang S et al. (2021) A deep learning algorithm using CT images to screen for coronavirus disease (COVID-19), Eur Radiol, https://doi.org/10.1007/s00330-021-07715-1.
166. Wang Y, Feng Z, Song L, Liu X, Liu S (2021) Multiclassification of Endoscopic Colonoscopy Images Based on Deep Transfer Learning", Computat Math Methods Med 2021:12. Article ID 2485934. https://doi.org/10.1155/2021/2485934
167. Xu X, Jiang X, Ma C, du P, Li X, Lv S, Yu L, Ni Q, Chen Y, Su J, Lang G, Li Y, Zhao H, Liu J, Xu K, Ruan L, Sheng J, Qiu Y, Wu W, … Li L (2020) A deep learning system to screen novel coronavirus disease 2019 pneumonia. Engineering 6(10):1122–1129. https://doi.org/10.1016/j.eng.2020.04.010
168. Yan Q, Wang B, Gong D, Luo C, Zhao W, Shen J, Ai J, Shi Q, Zhang Y, Jin S, Zhang L, You Z (2021) COVID-19 chest CT image segmentation network by multi-scale fusion and enhancement operations. IEEE Trans Big Data 7(1):13–24. https://doi.org/10.1109/TBDATA.2021.3056564
169. Yang M, Liu M, Chen Y et al (2021) Diagnostic efficacy of ultrasound combined with magnetic resonance imaging in diagnosis of deep pelvic endometriosis under deep learning. J Supercomput 77:7598–7619. https://doi.org/10.1007/s11227-020-03535-0
170. Zebin T, Rezvy S (2021) COVID-19 detection and disease progression visualization: deep learning on chest X-rays for classification and coarse localization. Appl Intell 51(2):1010–1021. https://doi.org/10.1007/s10489-020-01867-1
171. Zhang H, Zhang JS, Zhang HH, Nan YD, Zhao Y, Fu EQ, Xie YH, Liu W, Li WP, Zhang HJ, Jiang H, Li CM, Li YY, Ma RN, Dang SK, Gao BB, Zhang XJ, Zhang T (2020) Automated detection and quantification of COVID-19 pneumonia: CT imaging analysis by a deep learning-based software. Eur J Nucl Med Mol Imaging 47(11):2525–2532. https://doi.org/10.1007/s00259-020-04953-1